CALCITRIOL CONJUGATED QUANTUM DOTS, AN INNOVATIVE TOOL AS BOTH PROBE AND TREATMENT

by

Rachel Janine Schaefer

A thesis submitted to the Faculty of the University of Delaware in partial fulfillment of the requirements for the degree of Master of Science in Biological Sciences

Summer 2012

CALCITRIOL CONJUGATED QUANTUM DOTS, AN INNOVATIVE TOOL AS BOTH PROBE AND TREATMENT

by

Rachel Janine Schaefer

Approved: _____
Anja G. Nohe, Ph.D.
Professor in charge of thesis on behalf of the Advisory Committee

Approved: _____
Randall L. Duncan, Ph.D.
Chair of the Department of Biological Sciences

Approved: _____
George H. Watson, Ph.D.
Dean of the College of Arts and Sciences

Approved: _____
Charles G. Riordan, Ph.D.
Vice Provost for Graduate and Professional Education

ACKNOWLEDGMENTS

I would like to thank my family for providing me with the motivation, encouragement, patience, and financial support without which I would likely have never pursued a graduate degree. I would like to specifically thank my mother for her help over the years providing that desperately needed mental crutch such as after three all-nighters with an assignment due in just a few hours. I would like to thank my father for his advice and troubleshooting that would suddenly be required at the last minute, such as a time-consuming brake job or a malfunctioning computer. I would like to thank my sister for cheering me up, reminding me that the problem is not really as horrible or as important as it seems at the time.

I would like to thank my friend and mentor Jeremy for teaching me much of what I know about the lab now and supporting me by always willing to listen to my problems. His teamwork with composing a research paper and with several of my experiments helped them be successful. I would also like to thank both him and his wife, Kaitlyn, for letting me stay at their place while I completed the thesis.

I am thankful for Dr. Van Golen's help with the nude mouse injections and dissections. I would also like to thank him for allowing me to use his cell culture room and letting me use his SUM149 and MDA-MB-231 cell lines.

I would like to thank my committee members, Dr. Jia Song and Dr. Donna Woulfe for their help and suggestions for developing my thesis. They have always been willing to provide me with the time and assistance I need for my committee meetings, thesis, and defense.

I would like to thank Dr. Jeff Caplan and Dr. Kirk Czymmek for their help with confocal imaging and analysis at the Delaware Biotechnology Institute. I would also like to thank Dr. Nick Menegazzo and Dr. Karl Booksh for their help with managing the Fourier Transform Infrared Spectroscopy microscope and with analyzing the spectra.

I would like to thank the members of my lab for their help and encouragement throughout my time there. I would also like to thank my advisor, Dr. Anja Nohe for both her help and constructive criticism. I appreciate now having the independence necessary to really learn how to be a researcher. Having never been given the answers forced me to actually research to learn rather than having it just given by word of mouth. I also am pleased with having the ability to work in an interesting project on cancer research like I requested when we first met.

Lastly, I would like to thank the NIH and the Department of Biological Sciences at the University of Delaware for providing me funding through my graduate career.

TABLE OF CONTENTS

LIST OF FIGURES

ABSTRACT

Calcitriol is an essential Vitamin that has been extensively studied due to its potential role as therapeutic for many diseases, including breast cancer. Previous research has indicated that Calcitriol has a negative effect against the metastasizing ability of Inflammatory Breast Cancer (IBC) cells. Calcitriol bound QDs are a novel probe that can be used to examine the distribution of Calcitriol *in vitro* and *in vivo.* They were used to examine Calcitriol's mode of entry into these cells. Their use as a probe has been achieved by examining the uptake of Calcitriol bound QDs into IBC cells, which decreases when either caveolae or clathrin mediated endocytosis is disrupted. The probe was also used to examine colocalization, which was found between caveolae and CalQDs, but not between clathrin and CalQDs. This indicated that while clathrin mediated endocytosis is necessary for Calcitriol to have a normal level of uptake, Calcitriol enters IBC cells via caveolae and not clathrin coated pits. CalQDs were also used for the formation of an *in vivo* probe that may target CalQDs to IBC cells in order to enhance Calcitriol's potential ability to work as a therapeutic. CalQDs were directly targeted to IBC cells by conjugating the SM3 clone of Mucin-1 antibodies with Calcitriol bound QDs. In this study, Calcitriol bound QDs were used as both a probe and to create a potential therapeutic that could be explored for use against IBC metastasis.

Chapter 1

INTRODUCTION

1.1 Calcitriol (1, 25 Dihydroxyvitamin D3)

Calcitriol is a seco-steroid with three free hydroxyl groups. It is the active form of Vitamin D essential in many biological processes. Vitamin D is required for biological processes such as calcium and phosphate homeostasis, neuromuscular function, and inflammation of tissue [2]. On the cellular level it regulates multiple functions such as inhibition of cell growth, insulin secretion, and immune function [2]. Calcitriol mediates its biological effects in tissues positive for the Vitamin D Receptor (VDR) that are mostly found in organs such as the kidney, bone, intestine, or parathyroid gland [3].

Only 10% of the serum concentration of Vitamin D3 is taken in from diet, while the remaining 90% is synthesized from 7-dehydrocholesterol to a precursor of Vitamin D3 due to exposure to UVB radiation on the skin [3, 4] (Figure 1.1). Isomerization causes the precursor to be converted to Vitamin D3, otherwise known as cholecalcioferol. Vitamin D3 binds to carrier proteins, which in most cases is Vitamin

D-binding protein (DBP), which allows the Vitamin to be hydrophilic for its transfer to the liver. In the liver, Vitamin D3 is enzymatically hydroxylated to 25-hydroxyvitamin D, otherwise known as Calcidiol. 25-hydroxyvitamin D is bound to a carrier protein, such as DBP and is then transported to the kidneys where the final hydroxylation takes place that allows the formation of 1,25-dihydroxyvitamin D3, or Calcitriol. As an active form of Vitamin D, Calcitriol, is able to mediate its biological effects in the kidney, or be transported attached to a carrier protein, such as DBP to the bone, intestine, or parathyroid gland to induce its effects there.

Calcitriol induces its effects through its involvement and regulation of multiple signaling pathways [3, 5, 6]. It can signal by inducing transcription at the nucleus or via rapid non-genomic pathways in the cytoplasm [3] (Figure 1.2). For signaling to occur in the nucleus, after Calcitriol enters the cell, the VDR is induced to translocate to the cytoplasm where it binds to Calcitriol [3] (Figure 1.2). The binding causes VDR to be phosphorylated, allowing a 9-cis-retinoid X receptor (RXR) to form a heterodimer with it [3] (Figure 1.2). Before binding to VDR, the RXR activity is enhanced by beta-arrestin-2 [7] (Figure 1.2). Beta arrestins are signaling scaffolds for downstream MAPK signaling, but also link receptors to clathrin mediated endocytsosis [8]. Beta-arrestin acts as an adapter to receptors and clathrin coated pits by binding to ap-2 in clathrin coated pits [7] (Figure 1.2). After the RXR is fully active and bound to VDR, the heterodimer translocates to the nucleus [3, 9] (Figure 1.2). There it acts as a transcription factor by binding to Vitamin D Response Elements (VDRE) [3, 10-12] (Figure 1.2). The activated VDRE either promote or prevent the

transcription of downstream proteins [10, 12]. Additionally, Calcitriol initiates non genomic signaling such as calcium uptake [5, 6]. Calcitriol enters the cell and binds to the membrane-associated rapid response steroid- binding receptor (MARRS), which mediates the non-genomic signaling at the membrane [5, 6].

1.2 Calcitriol 1, 25 Dihydroxyvitamin D3 and its Potential use as a Therapeutic Agent

Low serum levels of Vitamin D have been linked to increased risk from cancer, diabetes, hypertension, multiple sclerosis, osteoporosis, and other diseases [13-15]. Vitamin D deficiency can be linked to increased mortality in diseases, such as with the increase in mortality rate observed with colon cancer and cardiovascular disease [13]. Low Vitamin D levels can also be a major cause of the disease, such as Rickets and other bone diseases for which Vitamin D treatment is commonly used as a therapeutic [16]. Clinical trials have explored the use of Calcitriol and Calcitriol analogs in breast, prostate, and colon cancer [17]. In the clinical trials with prostate cancer, there was a significant decrease in PSA with high levels (2-2.5µg daily) of Calcitriol treatment, but the affect against the disease was very small for the large risk of hypercalcemia [17]. Calcitriol analog was used as a treatment for breast and colon cancer, but the disease was stabilized in only a small percentage of treated patients [17].

Healthy serum levels of Calcitriol are below 50 pg/ml, which is 0.12 nM [18]. Serum levels higher than this may result in hypercalcemia [19]. A dose of 0.25 µg of

Calcitriol can be taken safely daily as a treatment, while higher doses of 0.5 μg can lead to hypercalcemia [19]. Targeting Calcitriol directly to cancer sites could potentially increase its ability to treat cancer at small doses, while avoiding hypercalcemia.

1.3 Calcitriol and Inflammatory Breast Cancer

1.3.1 Inflammatory Breast Cancer

Although only 5 percent of breast cancer cases are inflammatory, with its aggressive nature and high mortality rate, Inflammatory Breast Cancer (IBC) is the most severe form of breast cancer [20]. Even with multimodal treatment only 40 percent of those treated with combined chemotherapy, radiation, and surgery survive past five years [20]. The symptoms first appear as inflammatory skin changes, or erythema on one or both breasts along with swelling of the affected breast [20, 21]. The symptoms can also include edema resulting from IBC tumors blocking the draining of the lymphatic channels [20, 21]. Because of its symptoms, IBC is often misdiagnosed as a dermal infection, such as mastitis, often resulting in delayed treatment.

IBC has a younger age of onset than other breast cancers with an average age of diagnosis at 55 years of age [21]. Both pre- and postmenopausal women are susceptible. Obese women with higher BMI and African Americans have an increased

risk of contracting IBC. African Americans tend to be diagnosed at a much younger age with the average at only 48 years old, and have higher mortality rates with decreased survival times.

Most IBC tumors are triple negative, meaning that they do not express the Estrogen, Progesterone, and HER-2 receptors [21]. Unlike most metastatic tumors, they overexpress E-cadherin, rather than a loss in expression. This allows the cells to pile up into large emboli and metastasize into the lymphatic spaces. Treatments that prevent cell migration and break up or prevent the formation of emboli could be an effective treatment against IBC.

1.3.2 Inflammatory Breast Cancer and Calcitriol

Due to its potential as a therapeutic in other breast cancers, Calcitriol was explored by Hillyer, Sirinvasin, Joglekar, Sikes, Van Golen, and Nohe as a possible treatment against IBC [17, 22]. It had significant effects against IBC cell metastasis both *in vitro* and *in vivo* [22]. They tested a triple negative IBC cell line Sum149 against a non-inflammatory triple negative control, the MDA-MB-231 cell line [22]. They found that 100 nM Calcitriol had significant effects against the migration and invasion of SUM149 cell line, while not any significant effect against the non-inflammatory MDA-MB-231 cell line [22]. It also decreased the size of SUM149 emboli as compared to the non-treated control [22]. When nude immune deficient

mice were injected with SUM149 cells, those mice with cells treated with 100 nM Calcitriol before injection had less tumors metastasize to the lung [22].

1.4 Quantum Dots as a Probe

The distribution of Calcitriol in the organs and its signaling pathways have so far been examined indirectly, due the difficulty in producing antibodies against Calcitriol or developing a stable and biologically active fluorescently tagged probe. Since Calcitriol is a seco-steroid, it cannot be synthesized with Green fluorescent protein (GFP) tags in the cell. Therefore, most research has examined Calcitriol's location within cells indirectly by labeling associated proteins. Radio-labeling of hormones has been used to examine hormones directly, but it is expensive and requires the use of specialized equipment and large sample sizes [23]. Moreover, radio-labeled probes cannot be used for real time imaging. Recent labeling of Calcitriol with fluorescent BODIPY has several disadvantages, such as a high susceptibility to photobleaching and the stability of the complex has not been clearly defined through experimentation [23]. Quantum Dots (QDs) are semiconductor nanoparticles that are fluorescent under UV light [24]. Their high photo stability, brightness, and narrow range of emission make them desirable for imaging on a fluorescent microscope [24-26]. The use of nanoparticles synthetized in a variety of sizes and shapes made it possible by the development of advanced chemistry and the controlled synthesis of semiconductor QDs. The biofuntionalized particles have

surface chemistries that are compatible with the aqueous environment of living cells. Therefore, it is possible to track their movement and interactions with specific molecular targets in the cell membrane, cytoplasm and nucleus. These specialized imaging tools can be used to probe cell signaling pathways and detect cellular responses to signals [27]. The toxicity of QDs depends on their stability and coating [28]. If the QD degrades, then the cadmium core can be toxic. However if the coating is non-toxic and the QD is stable, then the QDs have a greatly decreased toxicity. The QDs used in this study have a cadmium selenide core with a zinc sulfide shell, however they are coated with non-toxic polymer carboxyl groups. According to the manufacturer, the toxicity of these particular QDs has not been confirmed *in vivo*.

1.5 Calcitriol bound Quantum Dots

Our previous research found that Calcitriol could be conjugated to QDs to develop a biological active fluorescent Calctriol probe (CalQDs) [1]. Using Fourier Transform Infrared Spectroscopy (FTIR), it was shown that Calcitriol remained coupled to QDs for three days at 4°C and 20°C, and for two days at 37°C [1]. This confirmed that they could remain stable for *in vitro* experiments performed at lower temperatures, such as examining low temperature uptake and signaling and also at biologically relevant temperatures *in vitro* and *in vivo*. Atomic Force Microscopy (AFM) was used to show that the QDs do not aggregate for two days at 37°C [1]. The uptake of CalQDs was examined in mouse myoblast cells (C2C12). When added to

C2C12 cells, the probe entered the cell within 2 hours [1]. CalQDs have been specifically shown to be biologically active in its ability to signal Vitamin D Response Elements (VDRE) [1]. With Calcitriol bound QDs confirmed as a viable tool in live cell imaging, they can be used to view Calcitriol localization and dynamics, including its entry into the cell and nucleus.

QDs are conjugated to Calcitriol through an esterfication reaction between a hydroxyl group on Calcitriol and a carboxyl group on the coating of the QDs. DMSO is used as a solvent and N,N'-Dicyclohexylcarbodiimide (DCC) is used as a linker agent [1]. DCC can activate the carboxyl groups through an electrophilic substitution at the oxygen in the carboxyl group after the carboxyl group is deprotonated. The central carbon atom of DCC acts as a strong electrophile for the nucleophilic oxygen in the carboxyl group. This results in an ester bond between the carboxyl group and DCC, forming the intermediate O-acyl isourea. The nucleophilic oxygen in the hydroxyl group in Calcitriol attacks the intermediate at the carbonyl group, forming an ester bond between the hydroxyl group and the carboxyl group and the solute dicyclohexylurea.

1.5.1 Stability of Calcitriol bound QDs

FTIR was used to analyze the successful conjugation [1]. Due to low sample concentrations (nM range) reflectance spectra were collected using a FTIR

microscope. When Calcitriol is conjugated to QDs, a hydroxyl group from Calcitriol and a carboxyl group from QDs form an ester bond (Figure 1.3). This chemical formation can be observed through FTIR, through the loss of the carboxyl stretch absorbance peak at 1566 cm^{-1} seen in the spectra of QDs (Figure 1.4D). Also, both hydroxyl groups at the 1α and 3β position on a cyclohexane within the chemical are free when Calcitriol is not conjugated with QDs. In the FT-IR spectrum of 1,3-cylcohexanediol, an absorbance peak is found at 1710 cm^{-1} [29]. This peak does not occur on the FTIR spectrum of cyclohexanol, a substance with only one hydroxyl group [30]. This indicates that the loss of a free hydroxyl groups results in the loss of the peak at 1710 cm^{-1}. All spectra have an absorbance peak around 1650 cm^{-1} from the C=C alkene stretch. So, Calcitriol has two absorbance peaks centered at 1710 cm^{-1} and at 1654 cm^{-1} from the two hydroxyl groups and the alkene stretch (Figure 1.4C) and QDs has two absorbance peaks centered at 1642 cm^{-1} and at 1566 cm^{-1} from the alkene stretch and the carboxyl stretch (Figure 1.4D). When Calcitriol is conjugated to QDs, this is indicated on FTIR spectra by the loss of both the peak at 1710 cm^{-1} from the loss of a hydroxyl group and the peak at 1566 cm^{-1} from the carboxyl stretch. Due to size exclusion chromatography, unbound Calcitriol and QDs manufactured without the addition of DCC are samples of unbound QDs with two absorbance peaks; one at 1649 cm^{-1} from the alkene stretch and the other at 1562 cm^{-1} from the carboxyl stretch (Figure 1.4B). When conjugated with the proper procedure, Calcitriol bound QDs display only a single peak at 1657 cm^{-1} from the C=C alkene stretch (Figure 1.3A).

Hence, FTIR results indicate that the procedure reported induces binding of Calcitriol to carboxyl coated QDs.

A stable complex of Calcitriol bound QDs is necessary for sufficient time for visualization with fluorescence microscopy. The stability of the conjugation between Calcitriol and QDs was measured using FTIR [1]. Samples were stored at 4°C, 20°C, and 37°C for three days. When the binding between Calcitriol and QDs dissociated, the ester bond was broken. When this occurs, the IR spectra the single peak found at 1649 cm^{-1} reverted back to the double peak with one peak at 1541 cm^{-1} and a second peak at 1647 cm^{-1}. Calcitriol bound QDs stored at 4°C and 20°C had spectra with a single peak with a frequency varying from 1649 to 1655 cm^{-1}, which indicated that the binding is still stable for at least 72 hours (Figures 1.5.I and 1.5.II). At 24 and 36 hours, Calcitriol coupled QDs stored at 37°C remained stable with a single peak at 1649 cm^{-1} (Figures 1.5.III.A and 1.5.III.B). However, at 72 hours, the IR-spectrum for Calcitriol coupled QDs stored at 37°C degraded to a double peak at with one peak at 1541 cm^{-1} and a second peak at 1647 cm^{-1} (Figure 1.5.III.C). Therefore, Calcitriol bound QDs remain stable at 20°C and 4°C for at least three days, and at 37°C they remain bound for two days.

1.5.2 Biological Activity of Calcitriol bound QDs

For Calcitriol bound QDs to be a viable probe, the ester bond formed must occur at a hydroxyl group on Calcitriol that allows retention of biological activity.

Binding to the 1α group on Calcitriol has been shown to negatively impact biological activity, while binding to the 3β hydroxyl does not result in a significant loss of biological activity [23]. Binding of Calcitriol to Vitamin D Response Elements (VDRE) in the nucleus is the end point of the Calcitriol signaling in the nucleus. Reporter gene assays with the use of the VDRE element were used to measure activation of this signaling pathway [1]. Calcitriol binds to the transfected plasmids containing VDRE and luciferase, resulting in the transcription and translation of the reporter, luciferase. The amount of luciferase transcribed is equivalent to biological activity. The VDRE stimulated luciferase activity was normalized to PRL-luc stimulated luciferase activity, which is expressed an equivalent amount in all transfected cells, so it reflects the number of transfected cells. Calcitriol bound QDs show an amount of activity similar to cells stimulated with Calcitriol (Figure 1.6A and 1.6B). The activity was less with cells stimulated with QDs than with Calcitriol bound QDs and Calcitriol alone as a positive control (Figure 1.6A and 1.6B). This demonstrated that Calcitriol bound QDs induce more biological activity than QDs, and about the same biological activity as Calcitriol.

1.5.3 Uptake of Calcitriol bound QDs into Live Cells

Calcitriol is known to accumulate in the nucleus of cells to exert its genetic effects. To test the biological activity and the entrance of Calcitriol conjugated QDs into the cell, we used confocal microscopy [1]. After addition of Calcitriol bound QDs

to C2C12 cells for 2h, a z-stack was collected using the Zeiss Live 5 confocal microscope. Figure 1.7 shows representative projection images and image slices through C2C12 cells treated with Calcitriol bound QDs (CalQDs) at 0 and 2 hours. These images showed a high concentration of the fluorescent complex (Figure 1.7C). Cells treated with control QDs synthesized without Calcitriol (ConQDs) and untreated cells did not have significant green fluorescence (Figure 1.7B and 1.7A). These experiments confirm that the Calcitriol bound QDs enter C2C12 cells by 2 hours and that cells incubated with the control QDs show no significant uptake of them in the cytoplasm or nucleus. This indicates that the probe is stable and viable i*n vitro*, and therefore not an observation of QD uptake, but of CalQD uptake.

1.5.4 Size of Calcitriol bound QDs

One problem with QDs as imaging tools is their time dependent aggregation and formation of large clusters rendering the fluorescent probe inactive. Therefore we investigated if the Calcitriol bound QDs aggregate over time [1]. The size of control QDs at day 0 and for Calcitriol bound QDs stored for three days at 37°C was measured using Atomic Force Microscopy (AFM). Twenty-five nanoparticles from each sample were randomly selected and measured from the height channel denoting diameter of each particle. The control QDs from day 0 are 10.32 nm in diameter (Figure 1.8). At Day 1 and 2 the Calcitriol bound QDs stored at 37°C have a slightly larger diameter due to the calcitriol coating, with 16.82 and 12.78 nm in diameter

respectively (Figure 1.8). However at Day 3, the Calcitriol bound QDs have aggregated to a size of 71.6 nm in diameter resulting in loss of biological functionality (Figure 1.8). This shows that CalQDs do not aggregate for two days when stored at 37°C.

1.6 Caveolae and Clathrin Mediated Endocytosis

It is generally thought that as a hydrophobic molecule, Calcitriol enters the cell by diffusing through the membrane and that its free form in serum is the active form that is uptaken. This is known as the free hormone hypothesis [31]. However, in circulation, Calcitriol is mostly bound to the DBP, which is hydrophilic [31]. Potential receptors have been identified for DBP on macrophages, neutrophils, and trophoblasts, which uptake Calcitriol [31]. This indicates that the DBP bound Calcitriol binds to receptors on the membrane of these cells. Since not many studies have observed Calcitriol directly, its uptake into the cell has not been examined closely. It is possible that it may enter the cell through endocytosis, while remaining bound to the Vitamin D binding protein (DBP). Other steroids, such as Estrogen, Testosterone, Androgen, and 25-Hydroxyvitamin D3 have been demonstrated to have an endocytotic mechanism for uptake, which violates the free hormone hypothesis [31]. Research indicates that the membrane receptor megalin is involved in the uptake of Androgen, Estrogen, and 25-Hydroxyvitamin D3 by binding to their carrier proteins, which is sex hormone-binding globulin (SHBG) for Estrogen and Androgen

and DBP for 25-Hydroxyvitamin D3 [31]. Evidence also indicates that testosterone bound to SHBG is uptaken via endocytosis in the principal cells of the epididymis [31]. If other steroids enter cells via endocytosis, it is possible that Calcitriol uses a similar mechanism. It could enter cells via caveolae or clathrin mediated endocytosis.

1.6.1 Caveolae

Caveolae are invaginations in the plasma membrane that are involved with endocytosis and cell signaling [32]. Caveolae are made up of three structural proteins caveolin-1, 2, and 3 [33]. The caveolins bind to membrane domains heavy with sphingolipids and cholesterol [33]. Caveolae can bind to ligands, which can trigger them to pinch off by dynamin and be internalized into the cytoplasm [32, 33]. They are involved in cell signaling by acting as a scaffolding domain in the cytoplasm [34]. Caveolin-1 (CAV-1) is essential to the structure and function of caveolae, so its downregulation via siRNA against CAV-1 results in less caveolae. Loss of cholesterol through methyl-β cyclodextrin also disrupts caveolae [35].

1.6.1.1 VDR-GFP Colocalization with Caveolae

VDR colocalizes with caveolae when CAV-1 is stimulated with Calcitriol in skeletal muscle cells [36, 37]. Treatment with Calcitriol results in the translocation of VDR from the nucleus to the caveolae signaling scaffold where Src is located. The

colocalization of VDR allows Src downstream signaling. Since Calcitriol may be a ligand for CAV-1 and triggers VDR translocation to the caveolae, it is possible that it could also be internalized through receptor mediated endocytosis.

1.6.1.2 Caveolae and Cancer

There is a link between caveolae expression and cancer severity [38]. However, the significance of this correlation greatly varies by the type of cancer and even by cell type. Caveolae expression can act as a tumor suppressor or ocnogene depending on cell type [38].

For example in head and neck cell squamous cell carcinomas CAV-1 overexpression results in increased lymph node metastases [39]. It also results in increased prostate cancer tumor progression and metastasis, since treatment with siRNA against CAV-1 decreases androgen expression [40]. Treatment with siRNA against CAV-1 can also decrease the proliferation of metastatic lung cancer cells [38]. However, high expression of CAV-1 is an indicator of increased survival in patients with prostate and breast melanoma [41].

While CAV-1 expression is not found in normal epithelial cells from breast tissue, it can sometimes be found in invasive breast cancer tissue. For example, it was found in 30% of invasive breast carcinoma and 13.4% of invasive breast cancer cases [42]. CAV-1 was associated with the expression of basal markers, high histological grade, and negative expression of steroid hormone receptors [42]. However, its

expression in stromal cells in breast cancer patients appears in less severe cases and in some cases high levels resulted in less metastasis [42]. A possible determination of whether increased or decreased CAV-1 expression is correlated with increased patient prognosis may be whether the cell line has epithelial or mesenchymal markers. Tumor cell types that have characteristics similar to epithelial cells tend to have decreased CAV-1 expression, while mesenchymal like cells tend to overexpress CAV-1 [43].

Since CAV-1 expression can have a major effect on the ability of cancer cells to proliferate and metastasize, it could possibly affect a treatment's ability to act against a particular cancerous cell type. For example, over-expression of CAV-1 may impact the ability of Calcitriol to treat a particular cell type, such as its impact against the over-expressing SUM149 cells, when contrasted against the effect it has against MD-MBA-231 cells, which do not over-express CAV-1 [44].

1.6.2 Clathrin Coated Pits

Clathrin coated pits are buds on the membrane involved in endocytosis. Clathrin monomers are essential to holding the structure of the pit together [45]. Clathrin coated pits are formed when Eps15 recruits AP-2 to the membrane, which is an adapter protein that binds to cargo. When enough cargo binds, the clathrin coated pit forms to allow endocytosis of the cargo. Eps-15-EH29 is a dominant negative form of Eps-15, which when transfected prevents the formation of clathrin coated pits, since functional Eps-15 is required to recruit AP-2 [46]. Methyl-β cyclodextrin also disrupts

clathrin coated pits, by removing cholesterol from the cell membrane [35]. Clathrin coated pits are also involved in downstream signaling pathways. For example, when receptors in clathrin coated pits bind to ligands and are activated, they can enhance the activity of beta-arrestin-2, which can increase RXR activity [7, 8]. RXR is required for Calcitriol to translocate to the nucleus, so disruption of clathrin coated pits could prevent nuclear uptake of Calcitriol [3].

1.6.2.1 Megalin Endocytosis of 25 Hydroxyvitamin D3

25-Hydroxyvitamin D3 is the precursor to 1alpha, 25-Dihydroxyvitamin D3 (Calcitriol). It is converted from the precursor in the proximal tubule cells of the kidney. While general dogma states that Vitamin D as a hydrophobic steroid should diffuse right through the membrane, 25-Hydroxyvitamin D3 actually enters the proximal tubule cells via endocytosis through clathrin coated pits [47].

25-Hydroxyvitamin D3 remains bound to DBP, which binds to megalin or cubilin receptors allowing the endocytosis of the compound. DBP is degraded in the lysosome and then 25-Hydroxyvitamin D3 is converted to Calcitriol [47].

With a similar structure to its precursor, it is possible that Calcitriol also enters cells via an endocytotic mechanism. Calcitriol may enter through clathrin coated pits like its precursor, but it may enter via alternative mechanisms, such as caveolae.

1.6.3 Calcitriol bound QDs as a Probe to Determine Endocytosis

Since the uptake of Calcitriol into cells can be visualized via Calcitriol bound QDs, they can be used as a probe to examine the entry of Calcitriol into the cell. Decreased uptake when disrupting endocytotic pathways is an indicator that endocytosis is necessary for Calcitriol's mode of entry.

1.7 Calcitriol bound Quantum Dots targeted Directly to Inflammatory Breast Cancer Cells with Mucin-1 Antibodies

Mucin-1 (MUC1) is a glycoprotein that is expressed apically on the surface of epithelial cells [48]. The amount of O-linked glycosylation on MUC-1 often decreases in epithelial carcinomas such as breast and prostate as they increase in the severity of the metastasis [48, 49]. This characteristic allows it to be a target for cancer therapy. Antibodies against the underglycosylated form are used for this effect. The SM3 clone of MUC1 is a monoclonal antibody that is particularly good at targeting the hypoglycosylated MUC1 on breast carcinomas, while not targeting to normal breast tissue [49]. The HMPV clone of MUC-1 is a monoclonal antibody that can be used as a positive control since it targets all forms of MUC-1 [50]. Antibodies have been successfully conjugated to QDs with functional targeting ability [51]. In order to have a sufficient concentration of Calcitriol *in vivo* at the IBC tumor site, it is necessary to directly target Calcitriol to the tumor. Calcitriol bound QDs conjugated with SM3 antibodies would allow the treatment to be concentrated at the tumor site.

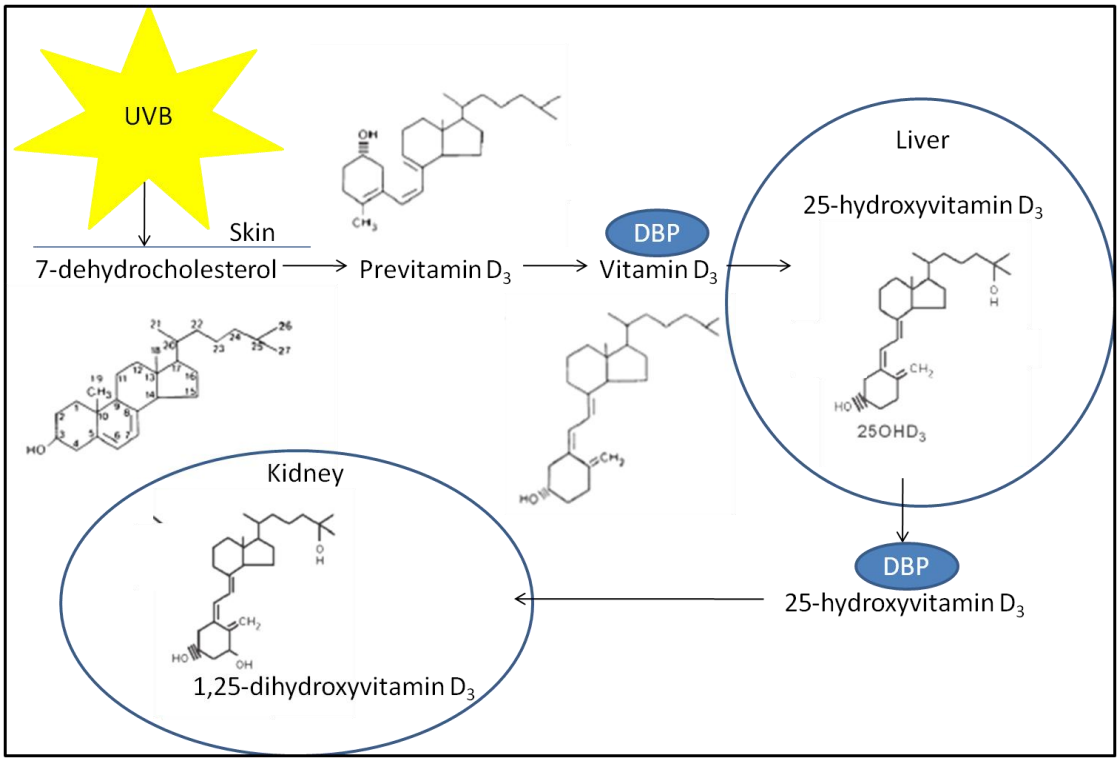

Figure 1.1 **Metabolism of Calcitriol from 7-Dehydrocholesterol. UVB radiation on the skin synthesizes pre-vitaminD3 from 7-dehydrocholesterol. Isomerization causes the precursor to be converted to Vitamin D3. Vitamin D3 binds to the Vitamin D-binding protein (DBP), which allow the Vitamin to be hydrophilic for its transfer to the liver. In the liver, Vitamin D3 is enzymatically hydroxylated to 25-hydroxyvitamin D. 25-hydroxyvitamin D is bound to DBP and is then transported to the kidneys where the final hydroxylation takes place that allows the formation of 1,25-dihydroxyvitamin D3, or Calcitriol. Picture adapted from [4].**

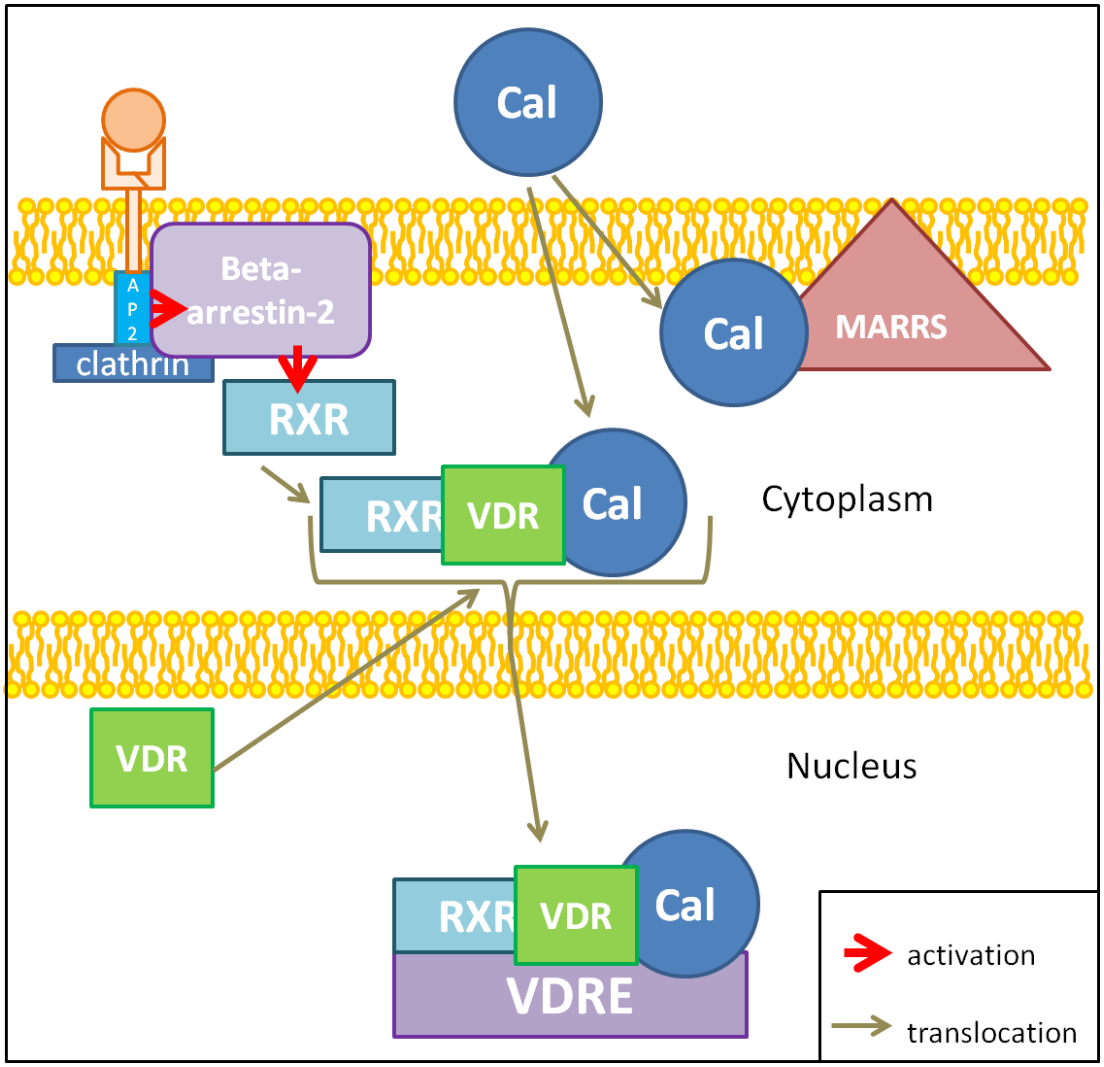

Figure 1.2 **Calcitriol Signaling Pathways. With a signaling pathway leading to downstream gene transcription and repression, after Calcitriol (Cal) enters the cell, the Vitamin D Receptor (VDR) is induced to translocate to the cytoplasm where it binds to Calcitriol. Before binding to VDR, the RXR activity is enhanced by beta-arrestin-2. Beta-arrestin acts as an adapter to receptors and clathrin coated pits by binding to ap-2 in clathrin coated pits. The retinoid X receptor (RXR) then forms a heterodimer with VDR after being activated. The heterodimer translocates to the nucleus where it acts as a transcription factor by binding to Vitamin D Response Elements (VDRE). With rapid response signaling in the cytoplasm, Calcitriol interacts with the membrane associated rapid response steroid binding protein (MARRS).**

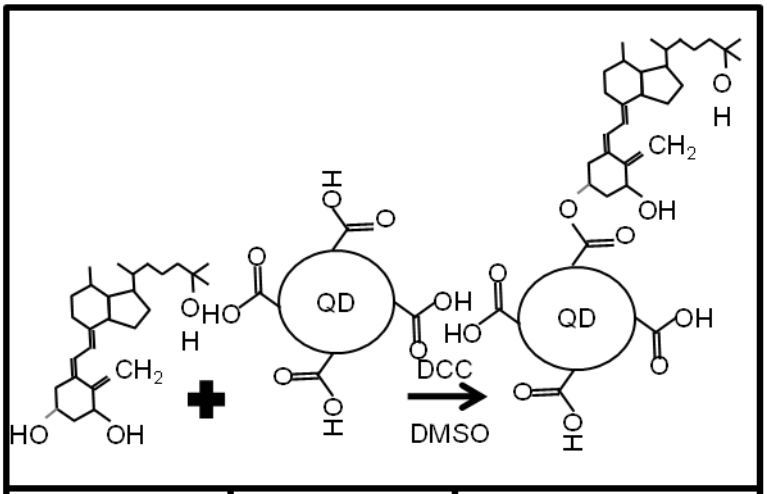

Calcitriol	QDs	Calcitriol bound QDs
FT-IR absorbance peaks in cm^{-1} (O-H stretch- 3395, C-H alkene stretch-2942, C-H alkane stretch 2872, O-H 1,3-2-cyclohexanediol 1710, C=C stretch 1654, C-O-H bending 1466, C-H alkane bend 1377)	FT-IR absorbance peaks in cm^{-1} (O-H stretch- 3323, C-H alkene stretch-2923, C-H alkane stretch 2853, C=C stretch 1642, Carboxyl stretch1566, C-O-H bending 1445, C-H alkane bend 1342)	FT-IR absorbance peaks in cm^{-1} (O-H stretch- 3352, C-H alkene stretch-2927, C-H alkane stretch 2856, ester stretch 1657, C=C stretch 1642, C-O-H bending and C-H alkane bend 1408)

Figure 1.3 The chemical structures showing the conjugation of Calcitriol bound QDs is displayed. Below the frequencies for the major FTIR absorbance peaks for the spectra are displayed for Calcitriol, QDs, and Calcitriol bound QDs. Published in [1].

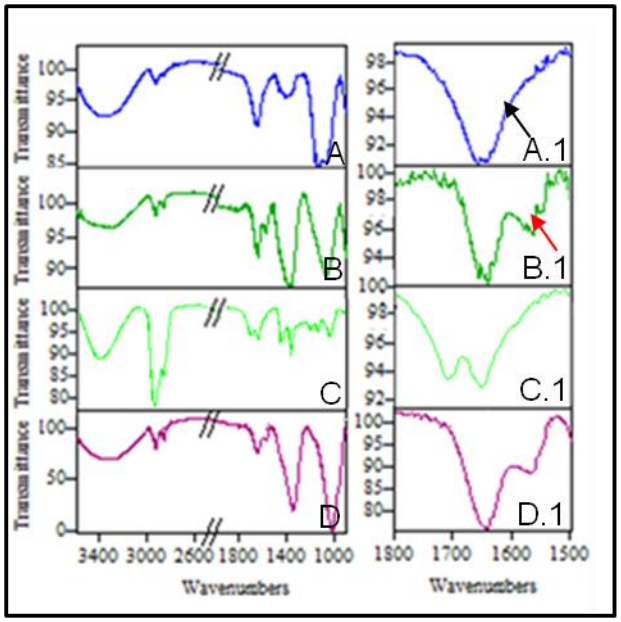

Figure 1.4 **FTIR Spectra of Calcitriol bound QDs, Unbound Calcitriol and QDs, Calcitriol, and QDs. Graphs A-D depicts the IR spectra of the samples from 3600-900 cm^{-1}. Graphs A.1-D.1 shows the IR spectra of the samples from 1800-1500 cm^{-1} where the indication of successful binding of Calcitriol to QDs, a single peak at 1650 cm^{-1} instead of a double peak at 1650 and 1550 cm^{-1} occurs. Spectra A and A.1 show the IR spectra of Calcitriol bound QDs. These samples were prepared with QDs, Calcitriol, and DCC. Spectra B and B.1 shows a sample prepared with QDs and Calcitriol without the necessary binding agent DCC. Spectra C and C.1 shows an IR spectra of the Calcitriol. Spectra D and D.1 shows an IR spectra of the QDs. Black arrows depict the single peak indicative of a successful conjugation of QDs to Calcitriol. A red arrow depicts the double peak indicative of unbound QDs and Calcitriol. Published in [1].**

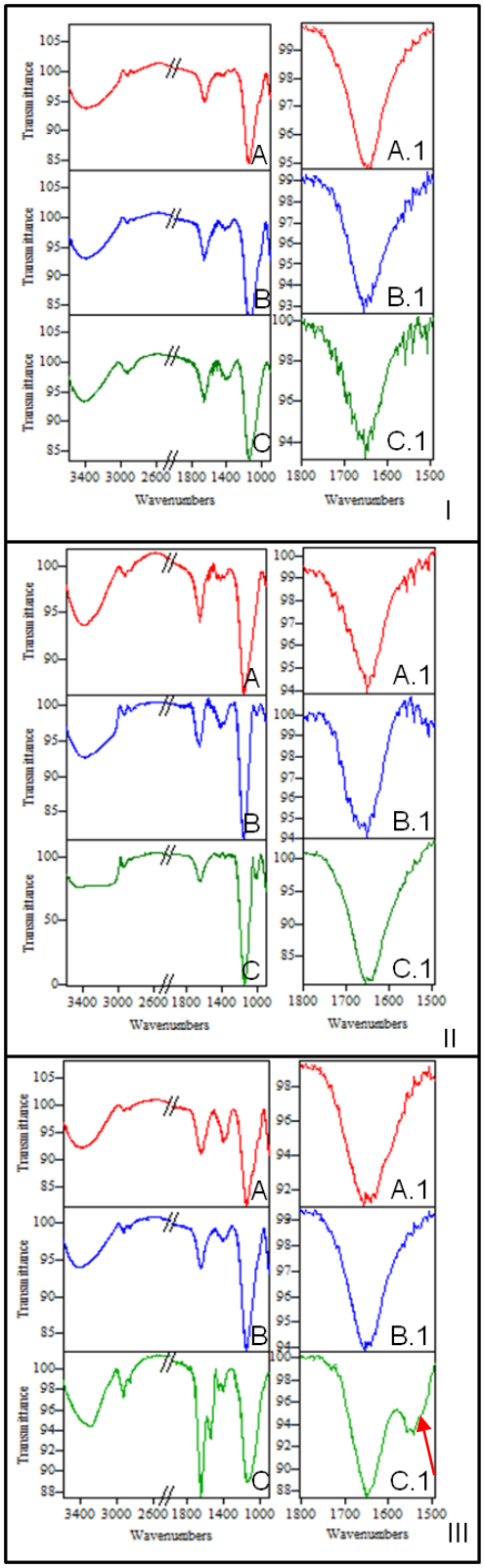
Transmittance
Wavenumbers
A
A.1
B
B.1
C
C.1
I
II
III

Figure 1.5 **FTIR Spectra of Calcitriol bound QDs over 3 Days at 4°C, 20°C, and 37°C. Graphs A-C depicts the IR spectra of the samples from 3600-900 cm^{-1}. Graphs A.1-C.1 shows the IR spectra of the samples from 1800-1500 cm^{-1} where the indication of successful binding of Calcitriol to QDs, a single peak at 1650 cm^{-1} instead of a double peak at 1650 and 1550 cm^{-1} occurs. All the graphs depict IR spectrum of samples that originally prepared from QDs, Calcitriol, and DCC that were placed at 4°C for section I, 20°C for section II, and 37°C for section III after a successful binding. Spectra A and A.1 shows the IR spectra at Day 1. Spectra B and B.1 shows the IR spectra at Day 2. Spectra C and C.1 shows the IR spectra at Day 3. A red arrow depicts the double peak indicative of unbound QDs and Calcitriol. Published in [1]**.

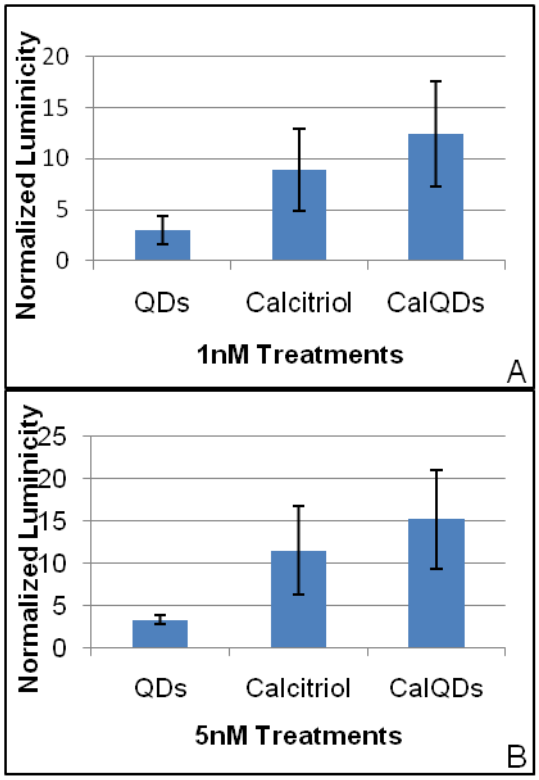

Figure 1.6 **Reporter gene assay showing biological activity of 1 nM and 5 nM Calcitriol, QDs, and Calcitriol bound QDs. The normalized reporter values of luciferase activity are shown with the standard error of the mean. Graph A shows the reporter values for C2C12 cells treated with 1 nM treatments. Graph B shows the reporter values for cells treated with 5 nM treatments. QDs represents the reporter values for cells treated with QDs. Calcitriol represents the reporter values for cells treated with Calcitriol. CalQDs represents the reporter values for cells treated with Calcitriol bound QDs. Published in [1].**

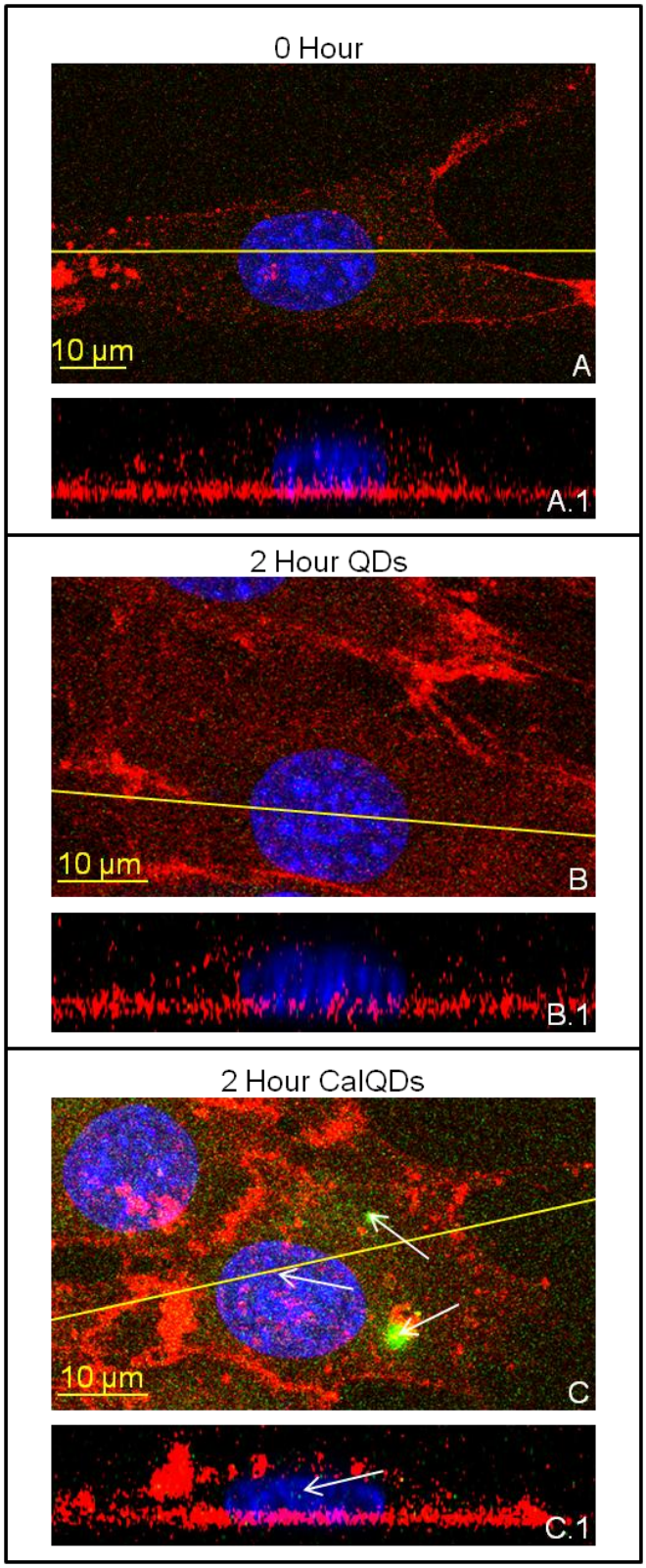
0 Hour
10 µm
A
A.1
2 Hour QDs
10 µm
B
B.1
2 Hour CalQDs
10 µm
C
C.1

Figure 1.7 **Confocal images of live C2C12 cells subjected to Calcitriol bound QDs or an unbound QD as control. Our data shows that Calcitriol bound QDs enter the cell and nucleus by 2 Hours. Projection images and slices were formatted in ImageJ imported into Corel PHOTO-PAINT X4. Z-stacks taken using the Zeiss LSM 510 VIS Confocal are displayed. A-C are projection images, while A.1-C.1 are slices taken vertically through the cell using Volume Viewer plug-in in ImageJ, displaying a side-view of the cell. Image A of the cells was left untreated and is labeled as 0 Hour. The cells treated with control QDs for 2 hours are displayed at image B. The cells treated with 1 nM Calcitriol bound QDs for 2 hours is displayed at image C. QDs is abbreviated for the 1 nM control QD treatment and CalQDs for the 1 nM Calcitriol bound QD. In the figure, the green denotes the QDs and Calcitriol bound QDs, the red denotes the membrane stain FM4-64, and the blue shows the nucleus stain Hoechst. White arrows depict the location of high concentrations of Calcitriol bound QDs. Published in [1].**

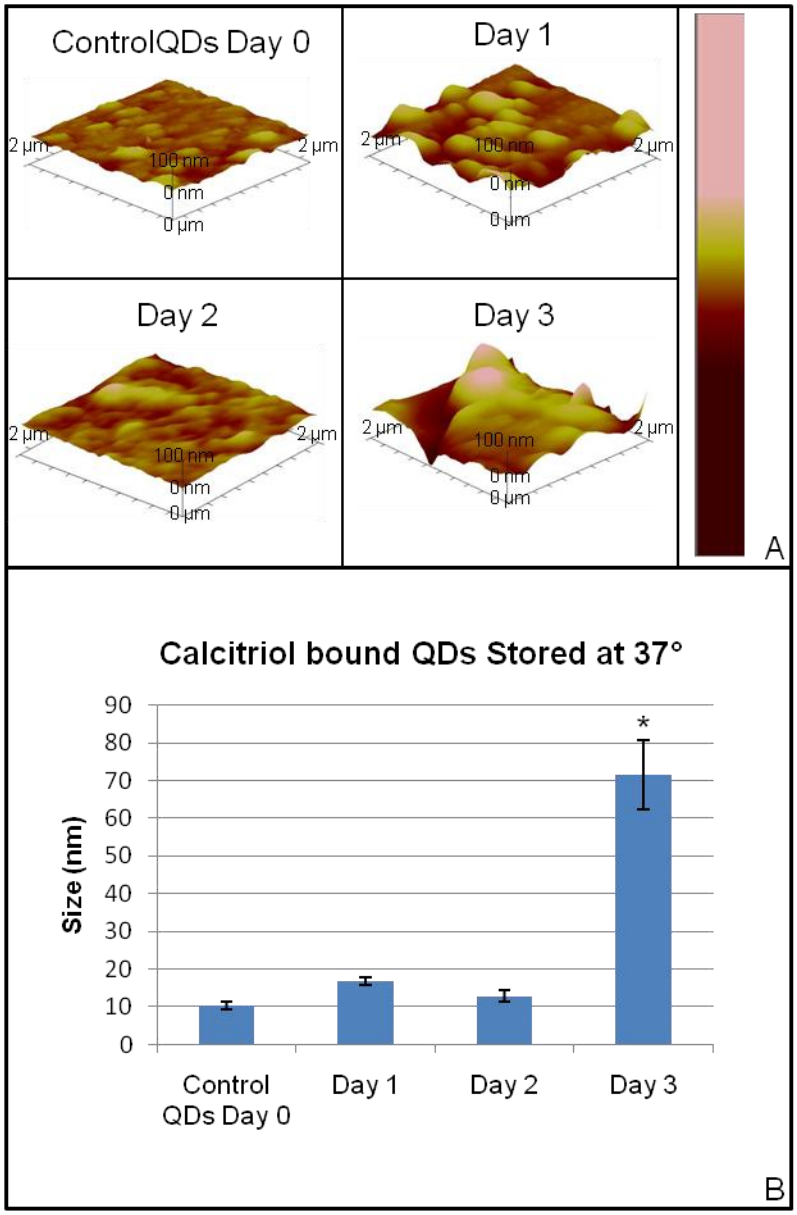

Figure 1.8 **Atomic force microscopy (AFM) was used to measure height of ControlQDs at day 0 and Calcitriol bound QDs that had been stored at 37°C over three days. CalQDs is abbreviated for Calcitriol bound QDs. Representative AFM images of each day were displayed starting on the day of Calcitriol bound QD synthesis (Day 0). B shows the average size of 25 randomly selected nanoparticles. The error bars display the S.E.M. * Significant compared to control QDs and Calcitriol bound QDs at Day 1 and 2, $p<.01$ as determined by ANOVA followed by Tukey's HSD post hoc test. Published in [1].**

Chapter 2

HYPOTHESIS AND AIMS

Hypothesis 1: Calcitriol bound Quantum Dots can be used as an imaging probe *in vitro* to better characterize the effect of Calcitriol on inflammatory breast cancer cells

Aim 1: Determine if Calcitriol enters inflammatory breast cancer cells via endocytosis through caveolae or clathrin coated pits

Aim 2: Determine if Calcitriol is biologically active in inflammatory breast cancer cells in the absence of caveolae or clathrin coated pits

Aim 3: Determine if there is Colocalization between Caveolae and Calcitriol and between Clathrin Coated Pits and Calcitriol.

Hypothesis 2: Calcitriol bound Quantum Dots can be used as treatment for inflammatory breast cancer via direct targeting through conjugation with SM3 Mucin-1 antibodies

Aim 1: Demonstrate that SM3 Mucin-1 Calcitriol bound Quantum Dots are specifically targeted to Sum149 cells *in vitro*

Aim 2: Demonstrate that HMPV Mucin-1 Calcitriol bound Quantum Dots are specifically targeted to inflammatory breast cancer tumors *in vivo*

Chapter 3

MATERIALS AND METHODS

3.1 Cell Culture

C2C12 (ATCC Manassas, VA) mouse myoblast cell lines are grown with DMEM media with 10% FBS, 1% L-Glutamine (Fisher Scientific, Pittsburg, PA), and 1% Penicillin/Streptomycin (100 IU/ml Penicillin, 100 µg/ml Streptomycin, Fisher Scientific, Pittsburg, PA) at 37°C and 5% CO_2.

SUM149 IBC cell lines are grown with Ham's F12 media with 5% FBS, 1% L-Glutamine (Fisher Scientific, Pittsburg, PA), .01% Hydrocortisone (Sigma-Aldrich, St. Louis, MO), 1% Antibiotic/Antimycotic (Gemini Bio-products, West Sacramento, CA) , 1% ITS Cocktail (Thermo Scientific HyClone, South Logan, UT), and 1% Penicillin/Streptomycin (100 IU/ml Penicillin, 100 µg/ml Streptomycin, Fisher Scientific, Pittsburg, PA) at 37°C and 5% CO_2.

3.2 Conjugation of Calcitriol to Quantum Dots

Qdot® 525 ITK™, Qdot® 605 ITK™, Qdot® 655 ITK™, and Qdot® 800 ITK™ and carboxyl quantum dots (QDs) were purchased from Invitrogen, Carlsbad, CA, 8 μM). Calcitriol was obtained from (Cayman Chemical Co., Ann Arbor, MI) dissolved in dimethylsulfoxide (DMSO, Fisher Scientific, Pittsburg, PA) to yield a 5 mM stock solution. N,N'-Dicyclohexylcarbodiimide (DCC, AnaSpec, Inc., Freemont, CA), was prepared in DMSO fresh as a 17 mM stock solution.

In order to conjugate Calcitriol to QDs, a 800 nM solution of QDs in PBS (pH 7.2) and 100 μM Calcitriol were mixed in a total volume of 50 μl of DMSO. 340 μM of DCC in DMSO was added to initiate the coupling process. As a control, unbound QDs, Calcitriol and DCC were mixed in the absence of Calcitriol. When additionally conjugated with antibodies, 50 μM of Calcitriol and 50 μM of SM3 Mucin-1 anti-human mouse antibody (eBioscience Inc., San Diego, CA) or HMPV Mucin-1 anti-human mouse antibody (BD Biosciences, San Jose, CA) are added in place of 100 μM Calcitriol. The reaction was carried out at room temperature for 30 minutes and excess DCC was removed by adding 100 μl of PBS. Separation of calcitriol linked QDs from unspecific reactants was achieved by size exclusion chromatography using Sephadex G-50 (Pharmacia Fine Chemicals St. Louis, MO) and sterile water.

3.3 Transfections

Cells were grown to 95% confluency before replacing media with media lacking serum (FBS). After 18 hours serum starvation, the media was changed to normal media and they were transfected or moch transfected with 2 µg of VDRE-luc (Promega, Madison, Wisconsin) and PRL-luc (Promega, Madison, Wisconsin) for reporter gene assays using Turbofect (Fermentas, Glen Burnie, ML) according to the manufacturers protocol. Some groups would be transfected with 2 µg of caveolin-1βGFP (CAV-1GFP), VDR-GFP, caveolin-1αRFP (CAV-1RFP), clathrinRFP, clathrinGFP, Eps15-EH29, or 10 µl siRNA against caveolin-1 (CAV-1) (Santa Cruz Biotechnology, Santa Cruz, CA) per 1.5 ml media. After four to six hours of transfection, the media is changed. Some groups are then treated with 5 nM methyl-β cycoldextrin (MBCD). After 24 hours the cells were stimulated with Calcitriol bound QDs, Calcitriol (Cayman Chemical Co. Ann Arbor, MI), or Control QDs (Invitrogen, Carlsbad, CA).

3.4 Reporter Gene Assay

After 24 hours after stimulation, cells were lysed with 1X Passive Lysis Buffer (Biotium, Hayward, CA). reporter gene assay was performed using the Firefly & Renilla Luciferase Assay Kit (30005-2) (Biotium, Hayward, CA). Luciferase activity was measured in triplicate using the MicroLumat LB 96P plate reader. Luminocity

values were calculated by averaging the three trials with the three triplicates, and normalizing to a non-stimulated control.

3.5 Live Cell Imaging

Cells were plated onto glass bottom dishes and grown to 95% confluency at 37°C and 5% CO_2 for two days. Cells were treated with 1 nM or 3 nM Calcitriol bound QDs (CalQDs) prepared as stated previously 2 hours before imaging. As a control, QDs not coated with Calcitriol were used (ConQDs). Some cell dishes were left untreated as the control. 20 minutes before imaging cells were stained with 20 µM of Hoechst 33342 (Thermo Scientific, West Palm Beach, FL) fluorescent nucleus stain. Directly before imaging, those cells not transfected with CAV-1GFP or VDR-GFP were stained with 158 µM Fm4-64 (Invitrogen, Carlsbad, CA) membrane stain. Images were taken using lasers of 405 nm wavelength for the Hoechst stain and 488 nm for the FM 464 stain and the green QDs or using lasers of 405 nm wavelength for the Hoechst stain, 488 nm for green CAV-1GFP or VDR-GFP, or 560 nm for the Infrared QDs, CAV-1RFP, and clathrinRFP. They were then imaged on the Zeiss LSM 510 Live5 Confocal Microscope and z-stacks of healthy cells were performed. Cells with good membrane and nucleus stains that best represent what was generally seen for each treatment were selected.

3.6 3D Imaging and Measurements

In LSM Image Examiner, selected z-stacks were made into projection images with all image slices put together into one image. ImageJ was used to create image slices of the selected z-stacks and to adjust the brightness and contrast of the images. A plug-in for ImageJ called Volume Viewer was used to create vertical image slices showing the side views of selected cells. The maximum and minimum displayed values of the channels were altered to better visualize the cells. The image slices were formatted in Coral PHOTO-PAINT X4 with an adjustment to the tone curve to enhance the brightness and contrast of the channels. The channel displaying QDs was set at a level to better display the difference between ConQD and CalQD treatments, so that ConQDs were set to show a very low intensity. The channel adjustments were kept constant for each figure, with the exception of the green CAV-1GFP channel of the CAV-1+siRNACAV-1+CalQDs in Figure 4.4A.2, which was adjusted to be 5X brighter so that the caveolae structure would be visible.

The z-stacks were put into Volocity 5.5, where they were made into three dimensional projection images with all image slices put together into one image. Volocity 5.5 was used to measure the mean pixel intensity of the CalQDs in the cytoplasm, which was calculated by subtracting the darkfeild from the mean intensities. Cytoplasmic and nuclear auto-fluorescence was subtracted from the green intensity values with the green 525 nm QDs (Invitrogen, Carlsbad, CA) and cytoplasmic and nuclear cross-talk from the green channel was subtracted from the red

channel with the red 655 nm QDs (Invitrogen, Carlsbad, CA). The control treatments with no QDs were set at zero by subtracting their mean intensity from each treatment.

Correlation and Colocalization was measured using the colocalization program in Volocity 5.5. Cells were selected and automatic thresholding was performed using the technique developed by Costes, Daelemans, Cho, Dobbin, Pavlakis, and Lockett [52]. Pearson's Correlation and Overlap Coefficient according to Mander's (M1 and M2) coefficients were measured. Background correlation and colocalization was subtracted from the measurements between VDR-GFP and CAV-1RFP and between VDR-GFP and clathrin-RFP.

3.7 QD Standard Curve of QDs on the IVIS Lumina

100 µl of QDs at 525 nm, 605 nm, 655 nm, and 800 nm at varying concentrations were placed in microcentrifuge tubes under the Vivo Vision IVIS Lumina (Xenogen) and imaged for 1 minute with small binning and a fluorescent Fstop of 4. They were imaged with the GFP/ICG emission excitation filters for 800 nm, the GFP/Dsred for 605 nm and 655 nm, and the GFP/GFP for 525 nm. ImageJ was used to measure the values of the pixels in the images taken, which was given as the intensity of the QDs.

3.8 Injection of CalQDs into Nude Mice with IBC tumors.

Nineteen 13-16 week old female Nude Immune Deficient Mice (Nu/nu) (Charles River, Wilmington, MA) were injected subdermally with SUM149 cells. After 6 weeks when tumors were visible, mice were tail vain injected with Infrared 800 nm 100 µl 40 nM Control QDs synthesized without Calcitriol, SM3 conjugated Calcitriol bound QDs, or Calcitriol bound QD. The synthesized particles were diluted with 10% 10x PBS and sterile water. Mice were imaged on the Vivo Vision IVIS Lumina (Xenogen) for 3 minutes with small binning and a fluorescent Fstop of 1 with the GFP/ICG emission excitation filters once a day for 3 days, then sacrificed on day 4. The liver, kidney, spleen, lungs, and tumors were isolated and imaged on the IVIS Lumina. Images were adjusted for brightness and contrast in ImageJ. The mean fluorescent pixel intensity of lungs and spleen was measured using the histogram function in ImageJ.

Chapter 4

RESULTS

4.1 Hypothesis 1 Calcitriol bound Quantum Dots can be used as an imaging probe *in vitro* to better characterize the effect of Calcitriol on inflammatory breast cancer cells

This study used three different treatments to disrupt caveolae and clathrin coated pits. Caveolae are specifically disrupted with the transfection of a plasmid encoding siRNA against caveolin-1 (siRNACAV-1), since caveolin-1 (CAV-1) is essential to the structure and function of caveolae. The formation of clathrin coated pits are specifically disrupted by the transfection of a plasmid expressing Eps-15-EH29 (EH29), a dominant negative form of Eps-15, since Eps-15 is only involved with clathrin coated pits, and functional Eps-15 is required to recruit AP-2 [46]. Caveolae and clathrin coated pits are both disrupted by the addition of methyl-β cyclodextrin (MβCD) to the cell media, which causes the removal of cholesterol from the membrane of cells [35].

4.1.1 Aim 1: Determine if Calcitriol enters inflammatory breast cancer cells via endocytosis through caveolae or clathrin coated pits

4.1.1.1 Calcitriol bound QDs are Taken up into the Cytoplasm by Two Hours

This study was done to determine where CalQDs are localized in the ccell, whether in the cytoplasm or nucleus, at 2 and 4 hours after the addition of CalQDs. This allows the selection of a time point that can be used to successfully observe CalQD uptake after treatment against endocytosis. In C2C12 mouse myoblast cells, CalQDs mean intensity was significantly greater in the cytoplasm at 2 hours and 4 hours as compared to at 0 hours, and there was a significantly higher intensity at 2 hours as compared to 4 hours (Figure 4.1A). This indicates that Calcitriol is significantly uptaken into cytoplasm of the cell by 2 hours, but is at a lower concentration in the cytoplasm by 4 hours. By 2 hours, the CalQDs mean intensity was significantly greater in the nucleus as compared to at 0 hours, but the intensity is significantly higher in the nucleus at 4 hours than at 2 hours (Figure 4.1B). This indicates that Calcitriol is significantly uptaken into nucleus of the cell by 2 hours, but is at a higher concentration in the nucleus at 4 hours. These results indicate that at 2 and 4 hour time points, Calcitriol has a higher concentration in the cytoplasm at 2 hours, and higher concentration in the nucleus at 4 hours. Since Calcitriol is generally located in the cytoplasm 2 hours after its addition, to determine the effect a treatment

has on Calcitriol uptake in the cytoplasm, observing the intensity of CalQDs at 2 hours is more effective than at 4 hours.

4.1.1.2 Expression of CAV-1GFP in SUM149 cells is Decreased when Treated with siRNA against Caveolin-1

This experiment was done to confirm the ability of siRNACAV-1 to knockdown the expression of CAV-1, which should specifically disrupt caveolae. When siRNACAV-1 was transfected in addition to a plasmid encoding CAV-1GFP, the mean intensity of CAV-1GFP was significantly less in SUM149 cells than the control cells transfected with CAV-1 alone (Figure 4.2). This demonstrates that the siRNACAV-1 treatment is successful in decreasing the expression of CAV-1. The EH29 and MβCD treatment did not show any significant difference in mean CAV-1 intensity compared to the control cells transfected with CAV-1 alone. Since EH29 and MβCD treatments do not function to affect the expression of CAV-1, but affect clathrin coated pits or disrupt caveolae structure, they did not have an effect on CAV-1 expression.

4.1.1.3 Calcitriol bound QD Uptake in SUM149 cells after Treatments against Caveolae and Clathrin Coated Pits is Decreased

This study was done to determine the role of endocytosis in Calcitriol uptake. Uptake of CalQDs into the cell was examined after disruption of caveolae and clathrin mediated endocytosis.

To successfully observe CalQD uptake in SUM149 cells, there must be significant difference in uptake of CalQDs compared to control ConQDs that are QDs not bound to Calcitriol. When SUM149 cells transfected with a plasmid CAV-1GFP were treated with CalQDs, there was a significantly higher mean intensity of CalQDs in the cytoplasm and nucleus compared to the intensity of cells treated with ConQDs (Figure 4.3). When the cells were only transfected with a control, there was a significantly higher mean intensity of CalQDs in the cytoplasm and nucleus as compared to the intensity of cells treated with ConQDs (Figure 4.3). These results indicate that CalQDs are uptaken significantly more than ConQDs in SUM149 cells non-transfected or transfected with CAV-1GFP, demonstrating that CalQDs are specifically uptaken, behaving differently from QDs alone. Therefore, CalQD treatment can be used to examine Calcitriol uptake when endocytosis is disrupted.

This experiment was done to observe CalQD uptake into cells when caveolae mediated endocytosis is disrupted by siRNACAV-1. When SUM149 cells transfected with CAV-1GFP were additionally transfected with siRNA against CAV-1 and treated with CalQDs, there was a significantly lower mean intensity of CalQDs in the

cytoplasm and nucleus of the cells when compared to the intensity in the cells of the CAV-1GFP CalQD treated group (Figure 4.4). This indicates that treatment with siRNACAV-1 decreases the uptake of CalQDs in the cytoplasm and nucleus. Therefore, caveolae function is necessary for Calcitriol uptake into the cytoplasm and nucleus.

This experiment was done to observe CalQD uptake into cells when clathrin mediated endocytosis is disrupted by EH29. When SUM149 cells transfected with CAV-1GFP were additionally transfected with eps-15-EH29 and treated with CalQDs, there was a significantly lower mean intensity of CalQDs in the cytoplasm and nucleus of the cells when compared to the intensity in the cells of the CAV-1GFP CalQD treated group (Figure 4.5). This indicates that treatment with EH29 decreases the uptake of CalQDs in the cytoplasm and nucleus. Therefore, clathrin coated pit function is necessary for Calcitriol uptake into the cytoplasm and nucleus.

This experiment was done to observe CalQD uptake into cells when both caveolae and clathrin mediated endocytosis is disrupted by MβCD. When SUM149 cells transfected with CAV-1GFP were additionally treated with MβCD and CalQDs, there was a significantly lower mean intensity of CalQDs in the cytoplasm and nucleus of the cells when compared to the intensity in the cells of the CAV-1GFP CalQD treated group (Figure 4.6). This indicates that treatment with MβCD decreases the uptake of CalQDs in the cytoplasm and nucleus. This confirms that both caveolae and

clathrin coated pit function is necessary for Calcitriol uptake into the cytoplasm and nucleus.

With all the treatments against caveolae and clathrin coated pits there was no significant difference in QD intensity between the treated groups with CalQD treatment and the untreated groups with ConQD treatment (Figures 4.4-4.6). This indicates that the treatments cause a close to complete disruption of the cells' ability to uptake CalQDs. This demonstrates that very little Calcitriol uptake occurs when caveolae or clathrin coated pits are disrupted.

4.1.2 Aim 2: Determine if Calcitriol is biologically active in inflammatory breast cancer cells in the absence of caveolae or clathrin coated pits

4.1.2.1 Calcitriol Biological Activity in SUM149 cells after Treatments against Caveolae and Clathrin Coated Pits is Decreased

The role of endocytosis in Calcitriol uptake was further examined by determining the biological activity of CalQDs after disruption of caveolae and clathrin mediated endocytosis. If CalQD uptake is prevented, then its biological activity should be similarly affected.

When the biological activity of Calcitriol was examined with a reporter gene assay, SUM149 cells transfected with VDRE and PRL-luc had significantly less luciferase activity when treated to disrupt caveolae with transfection of siRNA against CAV-1 as compared to just treated with Calcitriol (Figure 4.7). This indicates that

functional caveolae are necessary for Calcitriol induced biological activity. SUM149 cells transfected with VDRE and PRL-luc also had significantly less luciferase activity when treated to disrupt clathrin coated pits with transfection of eps-15-EH29 as compared to just treated with Calcitriol (Figure 4.7). This indicates that functional clathrin coated pits are necessary for Calcitriol induced biological activity. There was also significantly less luciferase activity when VDRE and PRL-luc trasfected cells were treated with methyl-β-cyclodextrin for use disrupting caveolae and clathrin coated pits as compared to just treated with Calcitriol (Figure 4.7). This confirms that functional caveolae and clathrin coated pits are necessary for Calcitriol induced biological activity. The results demonstrate that functional caveolae and clathrin coated pits are essential for normal Calcitriol uptake and biological activity, which could indicate that Calcitriol uses both caveolae and clathrin mediated endocytosis to enter the cell.

4.1.3 Aim 3: Determine if there is Colocalization between Caveolae and Calcitriol and between Clathrin Coated Pits and Calcitriol.

4.1.3.1 There is Increased Colocalization between VDR, caveolin-1, and Calcitriol bound QDs with the Introduction of Calcitriol bound QDs

This study was done to examine colocalization between Calcitriol, VDR, CAV-1, and clathrin. Endocytosis of Calcitriol in SUM149 cells is only possible if it colocalizes with the endocytotic structure in question *in vitro*. The colocalization was

determined by examining the images of SUM149 cells transfected with plasmids for the expression of VDRGFP and either CAV-1RFP or clathrinRFP for 2 hours after the addition of Calcitriol.

The Pearson's Correlation Coefficient is a measure of the strength of the linear dependence between two variables. The value can range from -1, which is a perfect negative linear correlation to 1, which is a perfect positive linear correlation. Absence of a linear relationship results in a value near 0. An increased Pearson's Correlation Coefficient in fluorescent images shows that there is a higher linear correlation between the pixel intensity distributions between channels, indicating increased correlation and a direct linear relationship between two different types of substances. The Overlap Coefficient according to Mander's measures the proportion of the intensity in each channel that coincides with the presence of some signal, regardless of intensity, in the other channel that is above the threshold value. The Overlap Coefficient according to Mander's ranges from 0, which is no overlap, to 1, which is a complete overlap of all the intensity in a channel overlapping with some of the other channel. An increase in Overlap Coefficient according to Mander's demonstrates that there is a higher proportion of a channel's signal that coincides with some of the other channel, indicating that a high proportion of one type of substance colocalizes with the other type of substance.

When CalQDs were added to SUM149 cells transfected with VDR-GFP and CAV-1RFP, there was an apparent increased correlation and colocalization between all three substances (Figure 4.8). This is visible with the appearance of white clusters

approaching the nucleus over 2 hours as seen in the image slices (Figure 4.8A). The white color is formed by the overlay of the red (caveolin-1), blue (CalQDs), and green (VDR) channels. There was additionally an increase in the Pearson's Correlation Coefficient and an increase in the Overlap Coefficient according to Mander's in each of the two way comparisons (Figure 4.8B). This indicates that when Calcitriol is added, Calcitriol colocalizes with caveolae and VDR. Therefore, it likely that Calcitriol is being uptaken at the caveolae in SUM149 cells.

However, when CalQDs were added to SUM149 cells transfected with VDR-GFP and clathrinRFP, there was only an increased correlation between VDR and clathrin (Figure 4.9). This is visible with the appearance of yellow clusters, rather than white in the cytoplasm as seen in the image slices (Figure 4.9A). The yellow color is formed by the overlay of the red (clathrin) and green (VDR) channels. There was additionally an increase in the Pearson's Correlation Coefficient in the two way comparison between VDR and clathrin, but not in the Overlap Coefficient according to Mander's (Figure 4.9B.1). This indicates that while increased levels of VDR may correlate with clathrin after Calcitriol treatment, the colocalization does not increase like with caveolae and VDR. There was no apparent correlation between CalQDs and clathrin or between CalQDs and VDR (Figure 4.9B.2-3). This indicates that Calcitriol does not colocalize with clathrin coated pits, which demonstrates that Calcitriol does not enter cells through clathrin coated pits. Although clathrin mediated endocytosis is necessary for Calcitriol uptake, it's possible that this is due to downstream signaling from clathrin coated pits.

4.2 Hypothesis 2 Calcitriol bound Quantum Dots can be used as treatment for inflammatory breast cancer via direct targeting through conjugation with SM3 Mucin-1 antibodies

4.2.1 Aim 1: Demonstrate that SM3 Mucin-1 Calcitriol bound Quantum Dots are specifically targeted to Sum149 cells *in vitro*

4.2.1.1 Calcitriol bound QDs conjugated with Mucin-1 Antibodies are Uptaken into SUM149 cells and are Biologically Active

The concentration of CalQDs necessary for the treatment of IBC is high enough to cause hypercalcemia [19, 22]. To target Calcitriol to IBC cells, CalQDs were conjugated with two clones of anti-human mouse Mucin-1 (MUC-1) antibodies. The SM3 clone of MUC-1 was used to target breast cancer cells, while the HMPV clone was used to target normal and cancerous epithelial tissue [49, 50]. Their uptake and biological activity was examined to confirm that their ability to enter cells and induce biological activity is at least as functional as CalQDs.

CalQDs and CalQDs conjugated with SM3 MUC-1 and HMPV MUC-1 antibodies had a significantly higher intensity of QDs in the cytoplasm and nucleus of SUM149 cells than the ConQDs (Figure 4.10). Also, the CalQDs conjugated with Mucin-1 had a slightly greater cytoplasmic and nuclear intensity than the CalQDs (Figure 4.10). A reporter gene assay experiment showed that the SM3 Mucin-1 Conjugated CalQDs (SM3 CalQDs) induce about as much luciferase reporter expression as CalQDs and Calcitriol, and had significantly more luciferase expression

than the ConQDs (Figure 4.11). These results indicate that CalQDs conjugated with MUC-1 antibodies are successfully uptaken into the cell and induce biological activity as well as CalQDs alone.

When the Mucin-1 Conjugated CalQDs were added to C2C12 cells, which are not targets of anti-human antibodies, they had a significantly greater cytoplasmic intensity of QDs ($p<.05$) than ConQDs, but the SM3 MUC1 CalQDs did not have a significantly greater intensity in the nucleus while the HMPV CalQDs intensity maintained significance compared to the ConQDs (Figure 4.12). The CalQDs had an even higher significantly greater intensity of QDs ($p<.01$) in the cytoplasm than the conQDs, and had also significantly higher QD intensity in the nucleus than the conQDs (Figure 4.12). This indicates that the MUC-1 conjugated CalQDs had a significantly lower uptake into the cytoplasm of C2C12 cells than the CalQDs, and the SM3 MUC-1 CalQDs had a significantly lower uptake in the nucleus than the CalQDs, which is likely due to the anti-human MUC-1 antibodies not targeting mouse cells.

4.2.2 Aim 2: Demonstrate that HMPV Mucin-1 Calcitriol bound Quantum Dots are specifically targeted to inflammatory breast cancer tumors *in vivo*

4.2.2.1 Calcitriol bound Infrared QDs conjugated with SM3 Mucin-1 Antibodies can be Examined *In Vivo* and Appear to be Targeted to the Lungs and Spleen

This study was done to examine the ability of SM3 MUC-1 to be directly targeted to IBC tumors *in vitro*. Nude immune compromised mice were treated with SUM149 cells. When the tumors were visible, the mice were injected with CalQDs, SM3 CalQDs, or ConQDs. The QDs with the highest fluorescent intensity were selected for the experiment.

QDs with four different emissions were tested for their visibility under the IVIS Lumina. The brightest QD type was selected for *in vivo* use. The QDs were conjugated to Calcitriol and the SM3 clone of MUC-1 used to target breast cancer cells and injected into nude immune compromised mice treated with SUM149 cells.

The 800 nm QDs had the highest fluorescent intensity under the IVIS Lumina (Figure 4.13). They reached pixel saturation at a 100 µl volume at 60 nM (Figure 4.13). However only 40 nM was used as a treatment in nude mice, and this is diffused throughout the mice after injection, so saturation of the *in vivo* images are unlikely.

When mice were treated with the QD treatments *in vivo*, in general mice with IBC tumors had a higher concentration of Infared QD treatment retained (Figure 4.14A). They appear to have been at their highest concentration at Day 2 (Figure 4.14A). At Day 2, CalQD and SM3 conjugated CalQD treatments appear to have been

concentrated in the lungs and spleen as compared to the Control QDs which had a more sporadic dispersal (Figure 4.14A). SM3 CalQDs were retained longer with more apparent at Day 3 than the other treatments (Figure 4.14A). At Day 2, the top view of the mice showed that mice treated with SM3 CalQDs and CalQDs had a significantly higher fluorescent intensity in the lungs in mice with visible tumors, than with mice with no tumors (Figure 4.14B). This indicates that SM3 CalQDs and CalQDs are present in the lungs at Day 2 mainly when tumors are present. At Day 2, the bottom view of the mice showed that mice treated with SM3 CalQDs had a significantly higher fluorescent intensity in the lungs in mice with visible tumors, than with mice with no tumors and that in mice with tumors there was a significantly higher intensity of SM3 CalQDs in the lungs than in mice treated with ConQDs (Figure 4.14C). This indicates that SM3 CalQDs, but not generally ConQDs, are present in the lungs at Day 2. At Day 2, the bottom view of the mice showed that mice treated with SM3 CalQDs and CalQDs had a significantly higher fluorescent intensity in the spleen in mice with visible tumors, than with mice with no tumors and that in mice with tumors there was a significantly higher intensity of SM3 CalQDs in the spleen than in mice treated with ConQDs (Figure 4.14C). This indicates that SM3 CalQDs and CalQDs, but not generally ConQDs, are present in the spleen at Day 2. These results indicate that when mice have IBC tumors developed from the SUM149 cells, mice injected with SM3 CalQDs have significantly more QDs in the spleen and lungs than mice treated with ConQDs. The spleens removed from the mice sacrificed four days after the treatments had a significantly higher fluorescence in all treatments when the mice had tumors

present (Figure 4.15). This further indicates that the presence of tumors impacts the distribution of QDs in organs.

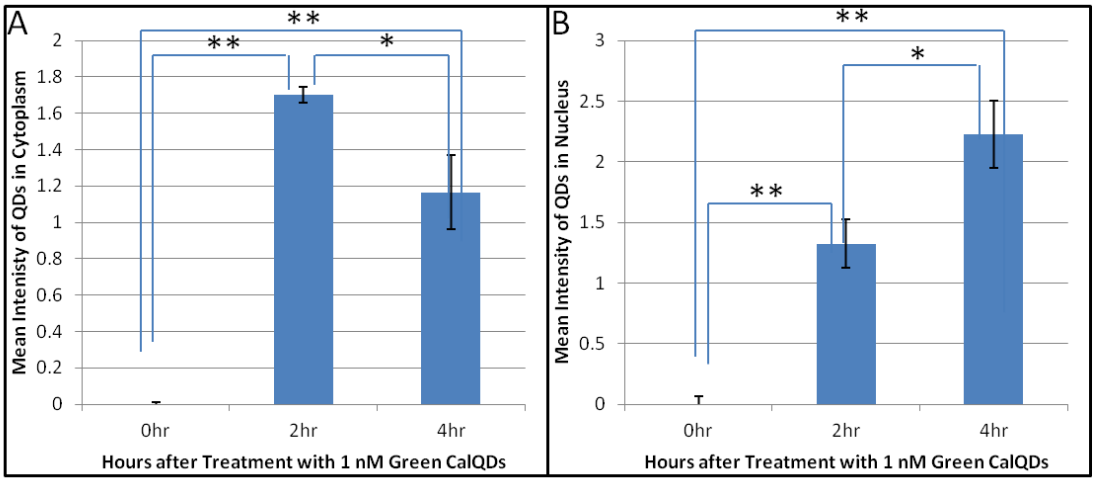

Figure 4.1 C2C12 cells were treated with 1 nM Green 525 nm Calcitriol bound QDs, for 2 or 4 hour intervals. The 0 hour treatment has no addition of Calcitriol bound QDs. Selected z-stack images were taken using lasers of 405 nm wavelength for the Hoechst stain, and 488 nm for the QDs and Fm4-64 membrane stain. A. Mean pixel intensity of the Calcitriol bound QDs observed in the cytoplasm of C2C12 cells for 0 hour, 2 hour, and 4 hour treatments. B. Mean pixel intensity of the Calcitriol bound QDs observed in the nucleus of C2C12 cells for 0 hour, 2 hour, and 4 hour treatments. The error bars display the S.E.M. * p<.05 ** p<.01 as determined by single factor ANOVA followed by Tukey's HSD post hoc test.

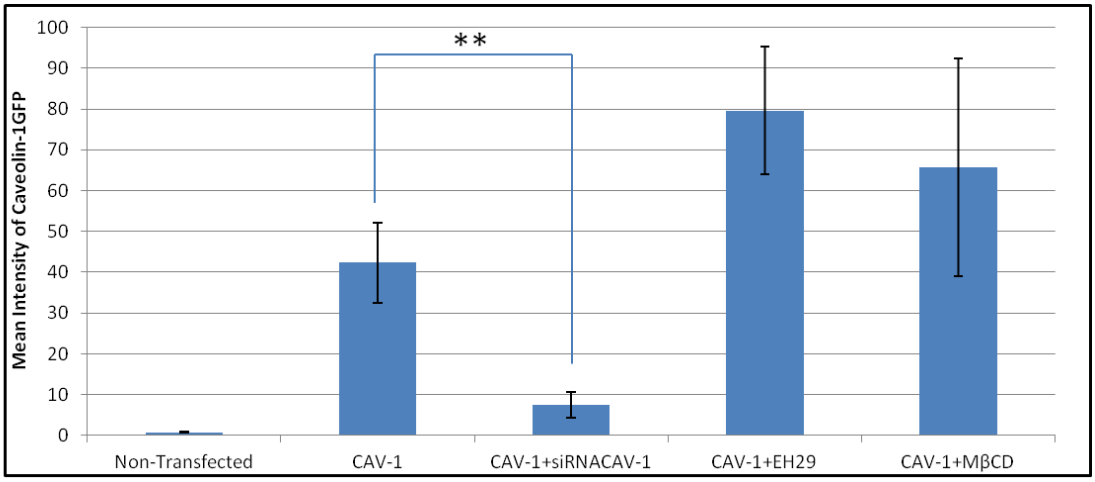

Figure 4.2 Mean Intensity of CAV-1GFP in SUM149 cells. Cells were transfected with CAV-1GFP, CAV-1GFP and siRNA against caveolin-1 (siRNACAV-1), and CAV-1GFP and Eps-15-EH29 (CAV-1+EH29). CAV-1GFP transfected cells were also treated with Methyl-β-cyclodextrin (CAV-1+MβCD). Non-transfected cells were examined as a control. Selected z-stack images were taken using lasers of 405 nm wavelength for the Hoechst stain, 488 nm for the CAV-1GFP transfection, and 561 nm for the 655 nm QDs. The mean pixel intensity of the CAV-1GFP in the cytoplasm of SUM149 cells is displayed. The error bars display the S.E.M. ** p<.01 as determined by unpaired two tailed t-test.

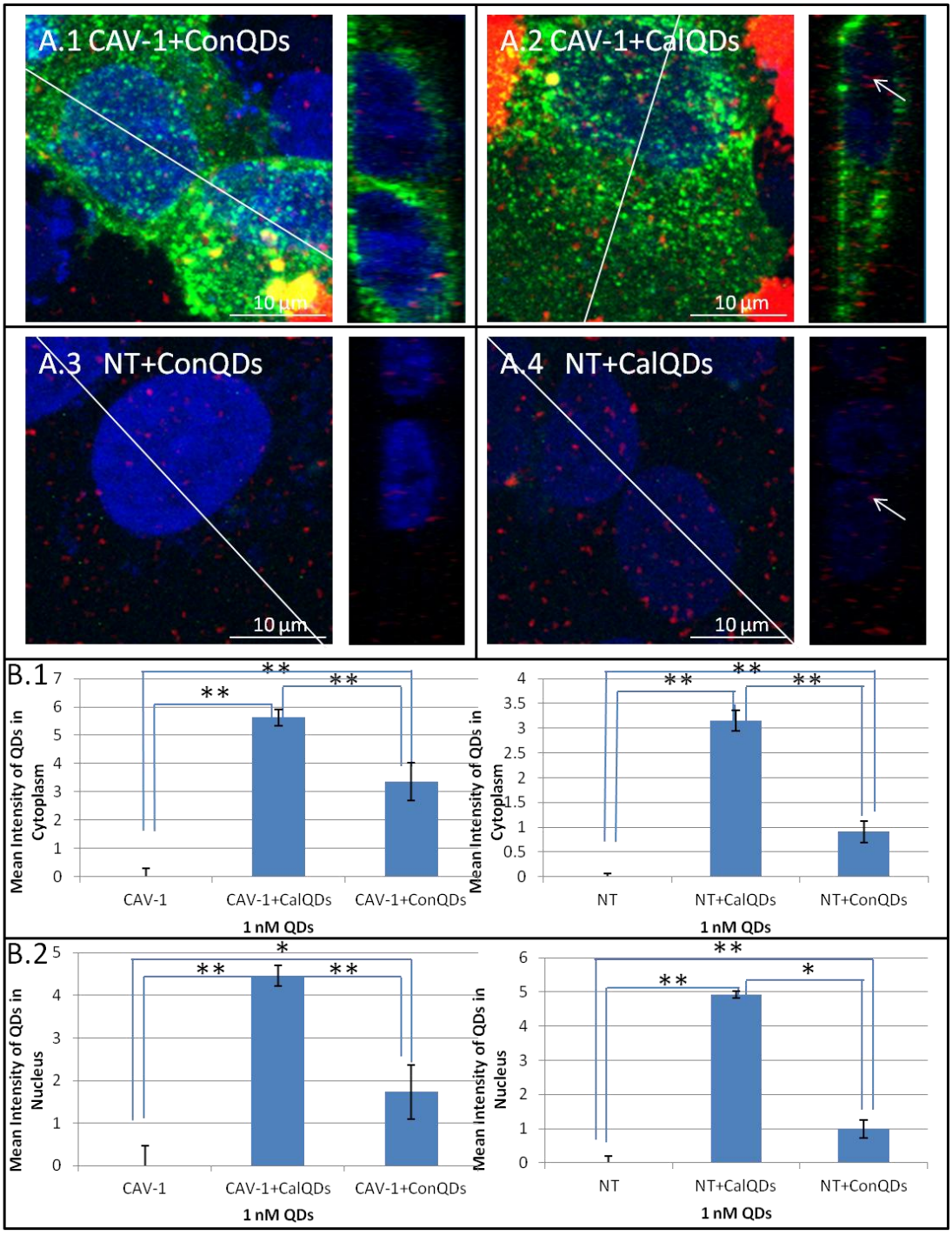
A.1 CAV-1+ConQDs
10 μm
A.2 CAV-1+CalQDs
10 μm
A.3 NT+ConQDs
10 μm
A.4 NT+CalQDs
10 μm
B.1
Mean Intensity of QDs in Cytoplasm
CAV-1
CAV-1+CalQDs
CAV-1+ConQDs
1 nM QDs
NT
NT+CalQDs
NT+ConQDs
1 nM QDs
B.2
Mean Intensity of QDs in Nucleus
CAV-1
CAV-1+CalQDs
CAV-1+ConQDs
1 nM QDs
NT
NT+CalQDs
NT+ConQDs
1 nM QDs

Figure 4.3 **Mean Intensity of Infrared Calcitriol bound QDs in SUM149 cells. Cells were transfected with CAV-1GFP (CAV-1) (A.1 and A.2) or a control transfection (NT) (A.3 and A.4). CAV-1 and Non-transfection groups were left untreated before imaging. The remaining groups were treated with 1 nM Infared 655 nm Control QDs (ConQDs) (A.2 and A.4) or CalQDs (CalQDs) (A.1 and A.3) for 2 hours before imaging. Selected z-stack images were taken using lasers of 405 nm wavelength for the Hoechst stain, 488 nm for the CAV-1GFP transfection, and 561 nm for the 655 nm QDs. A. The red channel displays the QDs, the green channel displays the CAV-1GFP, and the blue channel displays the nucleus. On the left are projection images, while displayed on the right are slices taken vertically through the cell, displaying a side-view of the cell. B. Mean pixel intensity of the CalQDs in the cytoplasm (B.1) and nucleus (B.2) of SUM149 cells. The error bars display the S.E.M. * $p<.05$ ** $p<.01$ as determined by single factor ANOVA followed by Tukey's HSD post hoc test. Arrows display large clusters of CalQDs.**

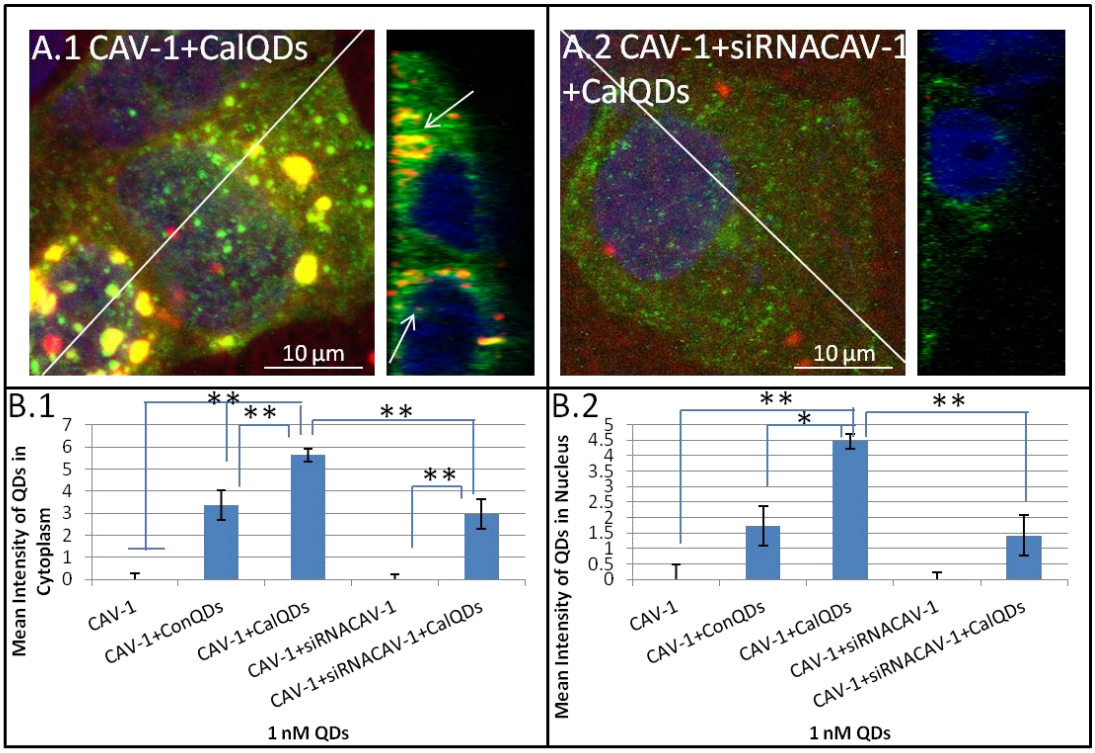

Figure 4.4 Mean Intensity of Infrared Calcitriol bound QDs in SUM149 cells after Downregulation or Disruption of CAV-1 or Caveolae. Cells were transfected with CAV-1GFP (CAV-1), or CAV-1GFP and siRNA against caveolin-1 (CAV-1+siRNACAV-1). Cells were left untreated or treated with 1 nM Infared 655 nm Control QDs (ConQDs) or Calcitriol bound QDs (CalQDs) for 2 hours before imaging. Selected z-stack images were taken using lasers of 405 nm wavelength for the Hoechst stain, 488 nm for the CAV-1GFP transfection, and 561 nm for the 655 nm QDs. A. The red channel displays the QDs, the green channel displays the CAV-1GFP, and the blue channel displays the nucleus. On the top are projection images, while displayed on the bottom are slices taken vertically through the cell, displaying a side-view of the cell. A.1. Displays the CAV-1+CalQDs treatment. A.2. Displays the CAV-1+siRNACAV-1+CalQDs treatment. The green CAV-GFP channel was adjusted to be 5X brighter so that the caveolae structure would be visible. B. The mean pixel intensity of the CalQDs in the cytoplasm (B.1) and nucleus (B.2) of SUM149 cells. The error bars display the S.E.M. * p<.05 ** p<.01 as determined by single factor ANOVA followed by Tukey's HSD post hoc test. Arrows display large clusters of CalQDs.

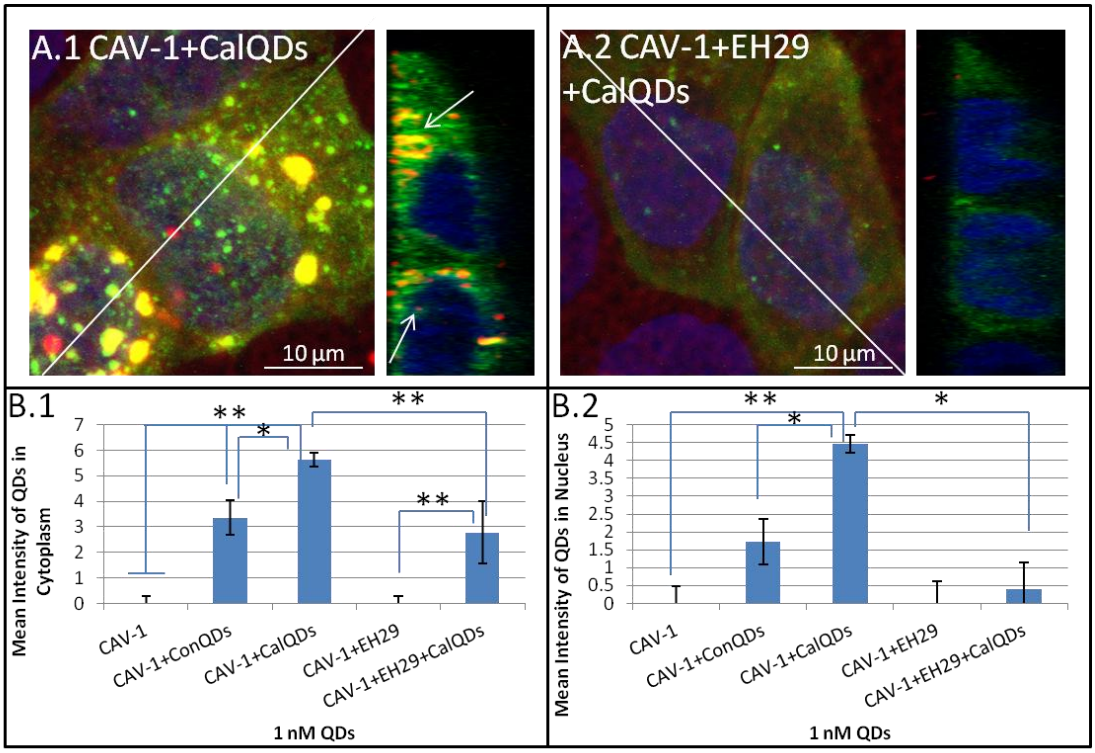

Figure 4.5 Mean Intensity of Infrared Calcitriol bound QDs in SUM149 cells after Disruption of Clathrin Coated Pits. Cells were transfected with CAV-1GFP (CAV-1), or CAV-1GFP and eps15-EH29 (CAV-1+EH29). Cells were left untreated or treated with 1 nM Infared 655 nm Control QDs (ConQDs) or Calcitriol bound QDs (CalQDs) for 2 hours before imaging. Selected z-stack images were taken using lasers of 405 nm wavelength for the Hoechst stain, 488 nm for the CAV-1GFP transfection, and 561 nm for the 655 nm QDs. A. The red channel displays the QDs, the green channel displays the CAV-1GFP, and the blue channel displays the nucleus. On the top are projection images, while displayed on the bottom are slices taken vertically through the cell, displaying a side-view of the cell. A.1. Displays the CAV-1+CalQDs treatment. A.2. Displays the CAV-1+EH29+CalQDs treatment. B. The mean pixel intensity of the CalQDs in the cytoplasm (B.1) and nucleus (B.2) of SUM149 cells. The error bars display the S.E.M. * p<.05 ** p<.01 as determined by single factor ANOVA followed by Tukey's HSD post hoc test. Arrows display large clusters of CalQDs.

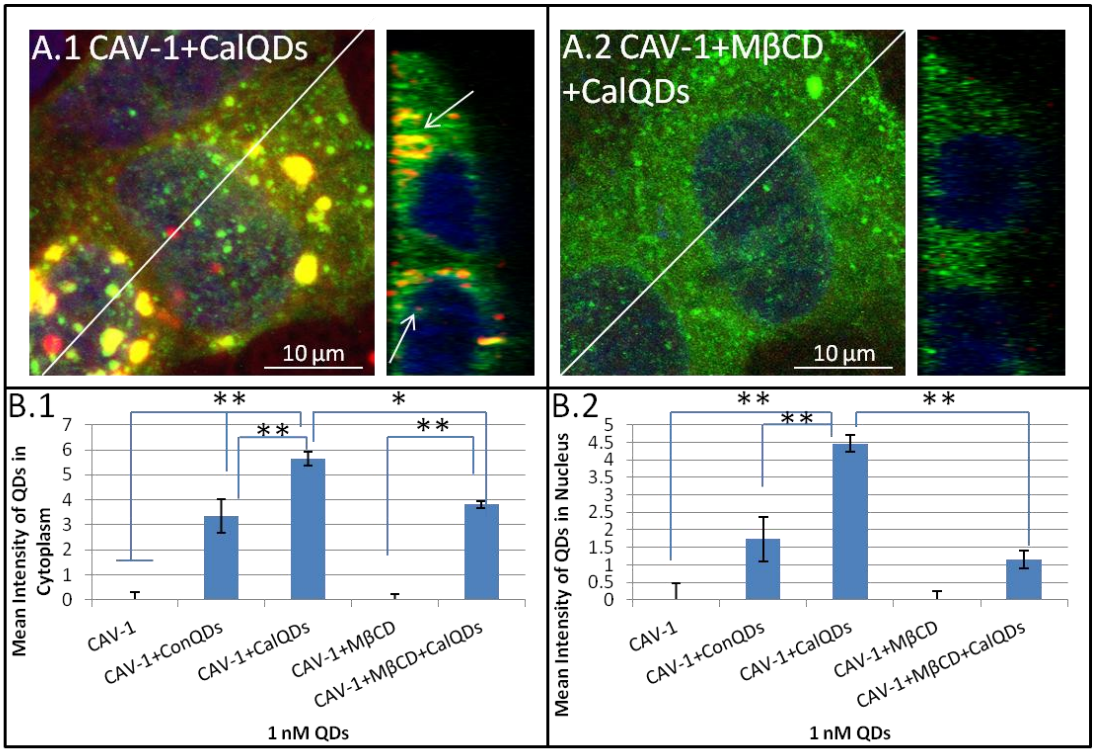

Figure 4.6 Mean Intensity of Infrared Calcitriol bound QDs in SUM149 cells after Disruption of Caveolae and Clathrin Coated Pits. Cells were transfected with CAV-1GFP (CAV-1), or additionally treated with methyl-β-cyclodextrin (CAV-1+MβCD). The cells were left untreated or treated with 1 nM Infared 655 nm Control QDs (ConQDs) or Calcitriol bound QDs (CalQDs) for 2 hours before imaging. Selected z-stack images were taken using lasers of 405 nm wavelength for the Hoechst stain, 488 nm for the CAV-1GFP transfection, and 561 nm for the 655 nm QDs. A. The red channel displays the QDs, the green channel displays the CAV-1GFP, and the blue channel displays the nucleus. On the top are projection images, while displayed on the bottom are slices taken vertically through the cell, displaying a side-view of the cell. A.1. Displays the CAV-1+CalQDs treatment. A.2. Displays the CAV-1+MβCD+ CalQDs treatment. B. The mean pixel intensity of the CalQDs in the cytoplasm (B.1) and nucleus (B.2) of SUM149 cells. The error bars display the S.E.M. * p<.05 ** p<.01 as determined by single factor ANOVA followed by Tukey's HSD post hoc test. Arrows display large clusters of CalQDs.

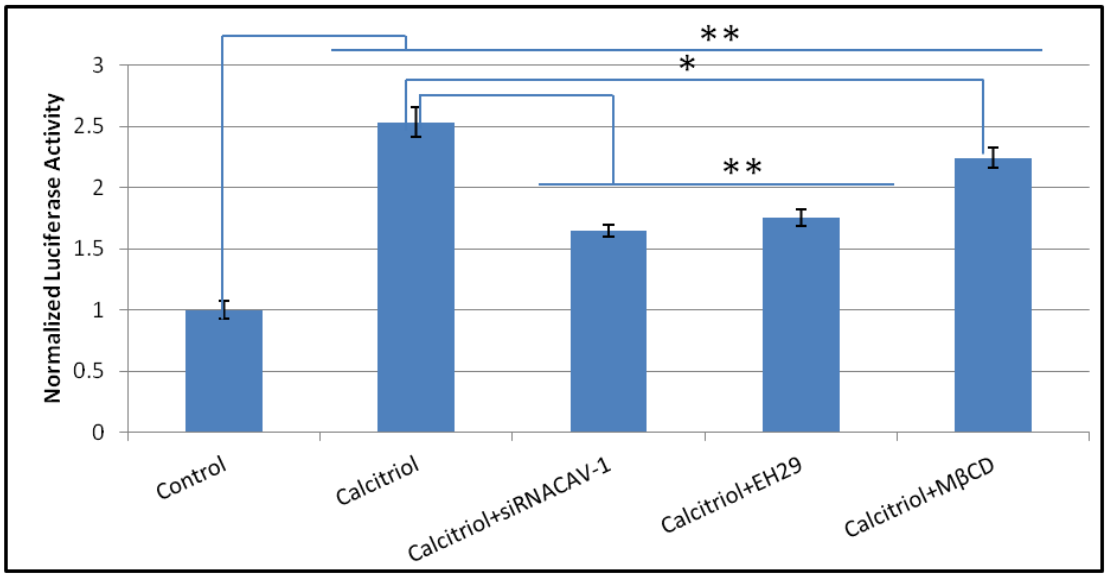

Figure 4.7 Reporter gene assay showing biological activity of 10 nM Calcitriol in cells treated for disruption of caveolae and clathrin coated pits. Cells were transfected with VDRE and PRL-luc and some groups additionally with siRNA against caveolin-1 (siRNACAV-1) or Eps-15-EH29 (EH29). Some groups of CAV-1 transfected cells were also treated with Methyl-β-cyclodextrin (MβCD). The Control was transfected with only VDRE and PRL-luc with no additional treatment. The normalized reporter values of luciferase activity are shown with the S.E.M. * p<.05 ** p<.01 as determined by single factor ANOVA followed by Fisher's LSD post hoc test.

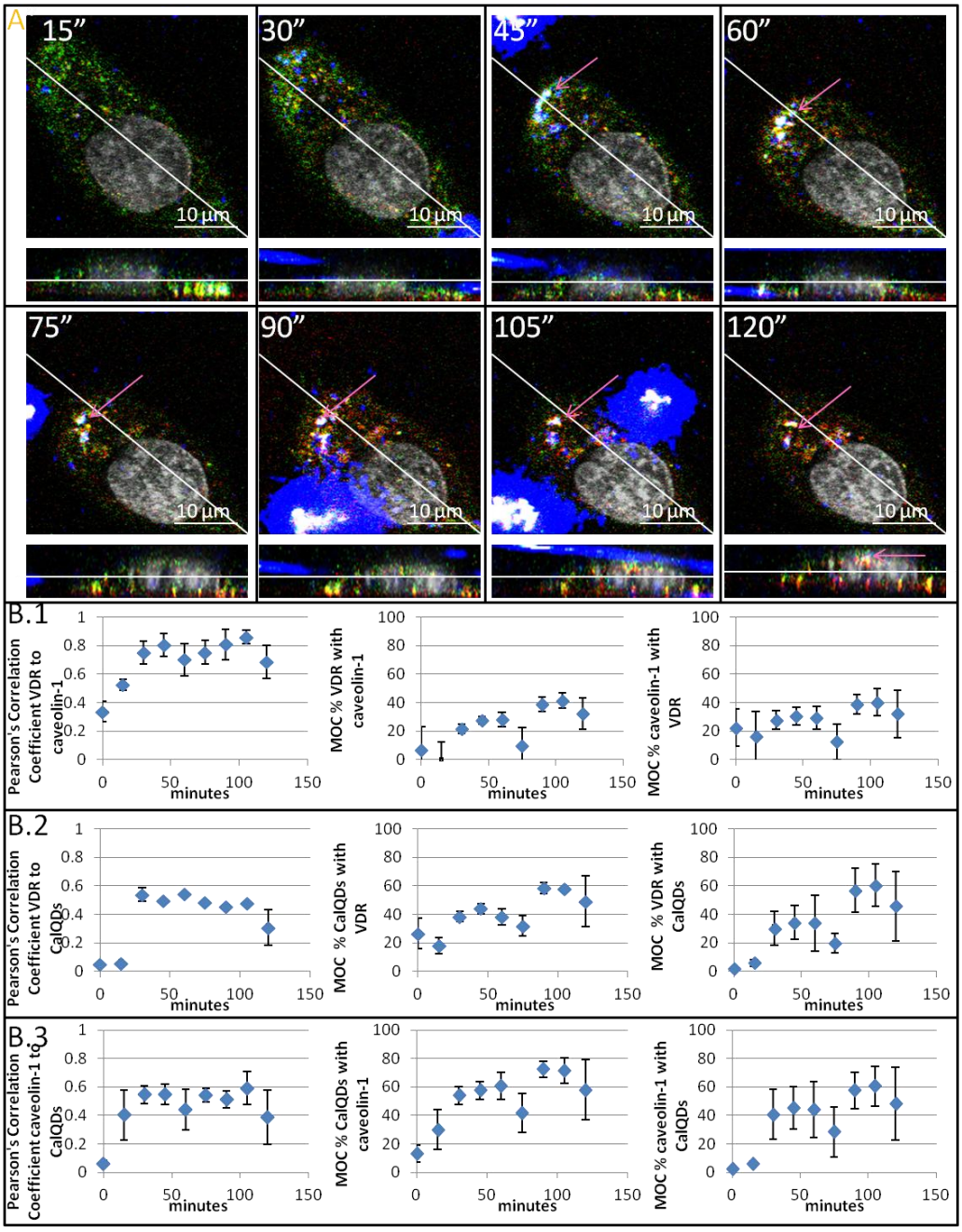
A
15”
30”
45”
60”
75”
90”
105”
120”
10 µm
B.1
Pearson's Correlation Coefficient VDR to caveolin-1
MOC % VDR with caveolin-1
MOC % caveolin-1 with VDR
B.2
Pearson's Correlation Coefficient VDR to CalQDs
MOC % CalQDs with VDR
MOC % VDR with CalQDs
B.3
Pearson's Correlation Coefficient caveolin-1 to CalQDs
MOC % CalQDs with caveolin-1
MOC % caveolin-1 with CalQDs
minutes

Figure 4.8 **Correlation and Colocalization between VDR-GFP and caveolin-1RFP and CalQDs over 2 Hours after treatment with 1 nM Infared CalQDs. SUM149 cells were transfected with caveolin-1RFP and VDR-GFP. Then they were treated with 1 nM Infared 655 nm Calcitriol bound QDs (CalQDs) for 2 hours, while a z-stack time series was taken with an image every 15 minutes. Selected z-stack images were taken using lasers of 405 nm wavelength for the Hoechst stain, 488 nm for the VDR-GFP transfection, and 560 nm for the caveolin-1RFP and QDs. A. The white channel displays the nucleus, the green channel displays the VDR-GFP, the red channel displays the caveolin-1RFP, and the blue channel displays the CalQDs. On the top are horizontal slices, while displayed on the bottom are slices taken vertically through the cell, displaying a side-view of the cell. B. Displays the Pearson's Correlation Coefficient and the Overlap Coefficient according to Mander's (MOC) to examine correlation and colocalization between VDR and caveolin-1 (B.1), VDR-GFP and CalQDs (B.2), and caveolin-1 and CalQDs (B.3). The error bars display the S.E.M. Arrows display large clusters of CalQDs colocalized with VDR and caveolae.**

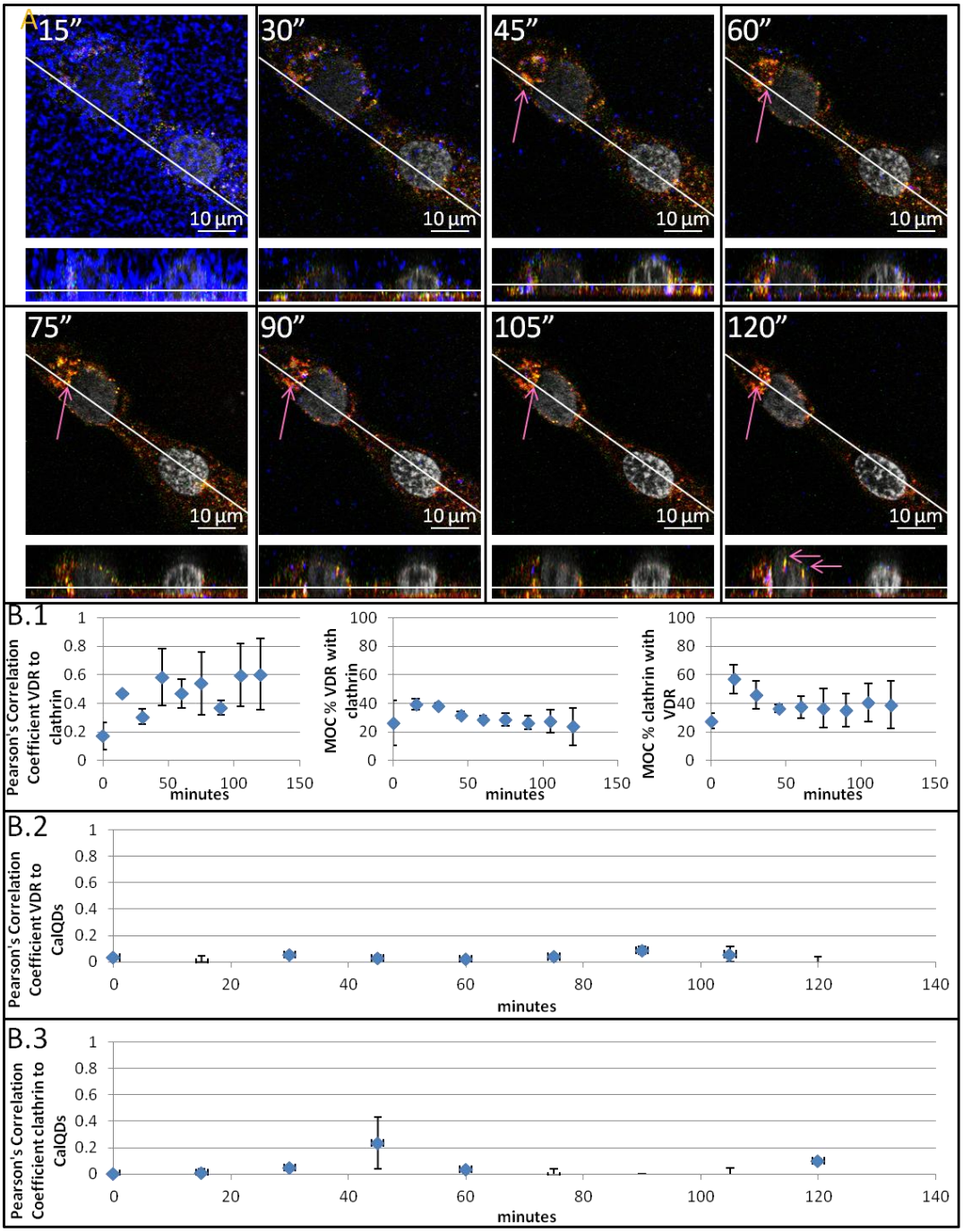
A
15”
30”
45”
60”
75”
90”
105”
120”
10 µm
B.1
Pearson's Correlation Coefficient VDR to clathrin
MOC % VDR with clathrin
MOC % clathrin with VDR
minutes
B.2
Pearson's Correlation Coefficient VDR to CalQDs
minutes
B.3
Pearson's Correlation Coefficient clathrin to CalQDs
minutes

Figure 4.9 **Correlation and Colocalization between VDR-GFP and clathrinRFP and CalQDs over 2 Hours after treatment with 1 nM Infared CalQDs. SUM149 cells were transfected with clathrinRFP and VDR-GFP. Then they were treated with 1 nM Infared 655 nm Calcitriol bound QDs (CalQDs) for 2 hours, while a z-stack time series was taken with an image every 15 minutes. Selected z-stack images were taken using lasers of 405 nm wavelength for the Hoechst stain, 488 nm for the VDR-GFP transfection, and 560 nm for the clathrinRFP and QDs. A. The white channel displays the nucleus, the green channel displays the VDR-GFP, the red channel displays the clathrinRFP, and the blue channel displays the CalQDs. On the top are horizontal slices, while displayed on the bottom are slices taken vertically through the cell, displaying a side-view of the cell. B. Displays the Pearson's Correlation Coefficient and the Overlap Coefficient according to Mander's (MOC) to examine correlation and colocalization between VDR and clathrin (B.1), VDR-GFP and CalQDs (B.2), and clathrin and CalQDs (B.3). The error bars display the S.E.M. Arrows display large clusters of CalQDs. Arrows display large clusters of VDR correlated with clathrin.**

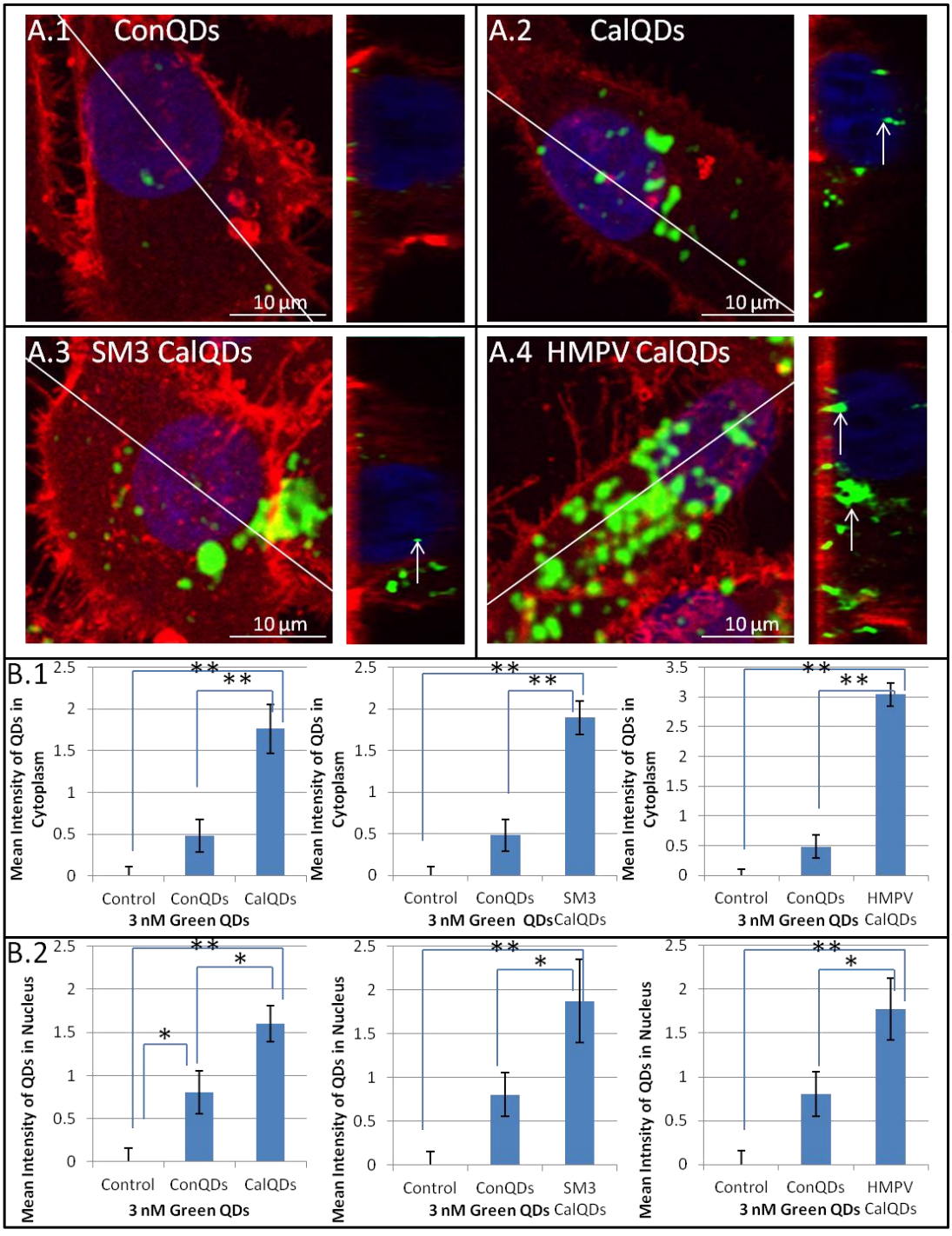
A.1 ConQDs
10 µm
A.2 CalQDs
10 µm
A.3 SM3 CalQDs
10 µm
A.4 HMPV CalQDs
10 µm
B.1
Mean Intensity of QDs in Cytoplasm
Control
ConQDs
CalQDs
SM3
HMPV
3 nM Green QDs
B.2
Mean Intensity of QDs in Nucleus
Mean Intntsity of QDs in Nucleus

Figure 4.10 **SUM149 cells were treated with 3 nM Green 525 nm Control QDs (ConQDs) (A.1), Calcitriol bound QDs (CalQDs) (A.2), Calcitriol bound QDs conjugated with Anti-Human SM3 Mucin-1 antibodies (SM3 CalQDs) (A.3), or Calcitriol bound QDs conjugated with Anti-Human HMPV Mucin-1 antibodies (HMPV CalQDs) (A.4) for 2 hours. The control treatment has no addition of QDs. Selected z-stack images were taken using lasers of 405 nm wavelength for the Hoechst stain, and 488 nm for the QDs and Fm4-64 membrane stain. A. The red channel displays the membrane stain, the green channel displays the QDs, and the blue channel displays the nucleus. On the left are projection images, while displayed on the right are slices taken vertically through the cell, displaying a side-view of the cell. B. Mean pixel intensity of the QDs in the cytoplasm (B.1) and nucleus (B.2) of SUM149 cells. The error bars display the S.E.M. * $p<.05$ ** $p<.01$ as determined by single factor ANOVA followed by Fisher's LSD post hoc test. Arrows display large clusters of QDs.**

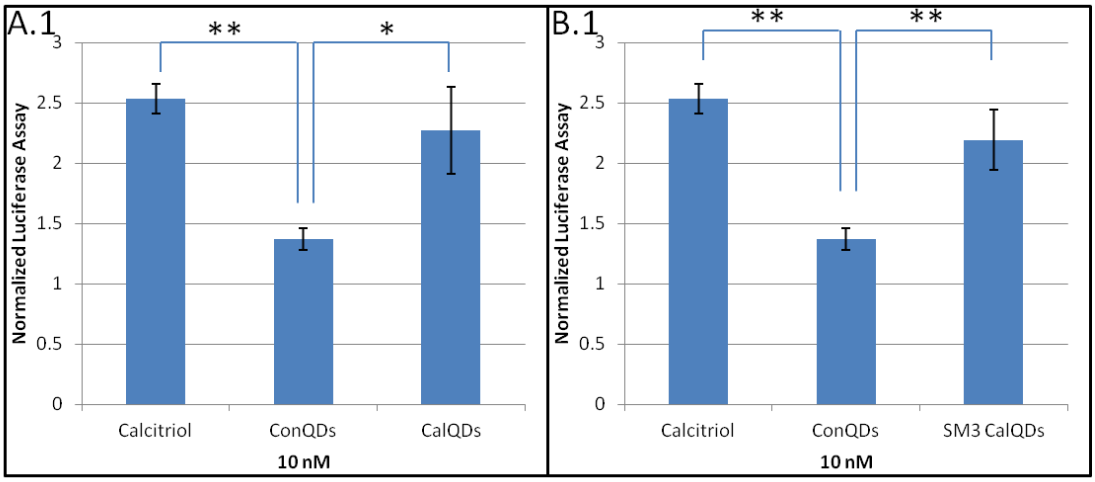

Figure 4.11 Reporter gene assay showing biological activity of Calcitriol in cells treated with 10 nM Calcitriol, Green 525 nm Control QDs (ConQDs), Calcitriol bound QDs (CalQDs), or Calcitriol bound QDs conjugated with Anti-Human SM3 Mucin-1 antibodies (SM3 CalQDs). Cells were transfected with VDRE and PRL-luc before stimulation with CalQDs. The Control was transfected with only VDRE and PRL-luc with no additional treatment. The normalized reporter values of luciferase activity are shown with the S.E.M. * p<.05 ** p<.01 as determined by single factor ANOVA followed by Tukey's HSD post hoc test.

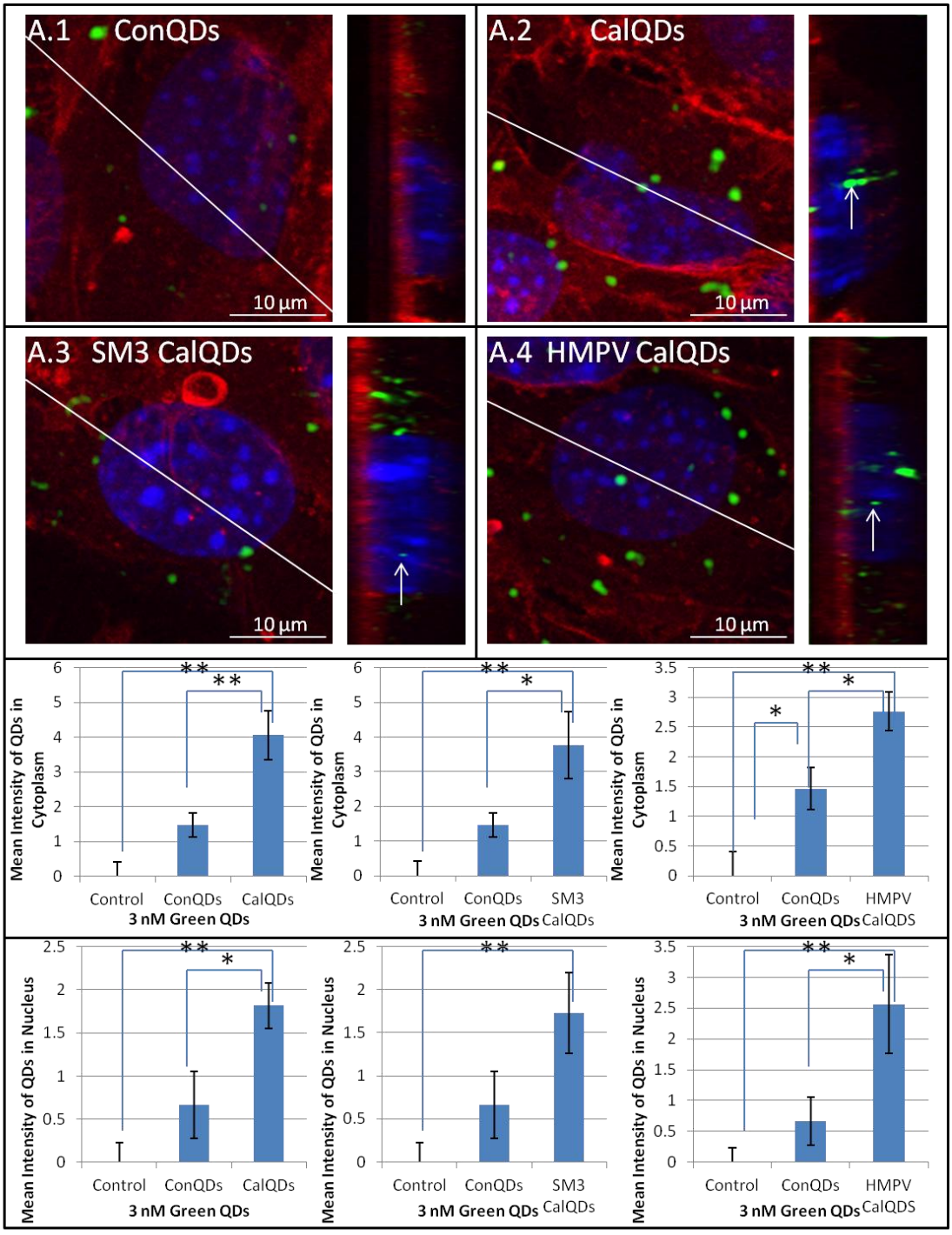
A.1 ConQDs
10 µm
A.2 CalQDs
10 µm
A.3 SM3 CalQDs
10 µm
A.4 HMPV CalQDs
10 µm
Mean Intensity of QDs in Cytoplasm
Control
ConQDs
CalQDs
SM3
HMPV
3 nM Green QDs
Mean Intensity of QDs in Nucleus

Figure 4.12 **C2C12 cells were treated with 3 nM Green 525 nm Control QDs (ConQDs) (A.1), Calcitriol bound QDs (CalQDs) (A.2), Calcitriol bound QDs conjugated with Anti-Human SM3 Mucin-1 antibodies (SM3CalQDs) (A.3), or Calcitriol bound QDs conjugated with Anti-Human HMPV Mucin-1 antibodies (HMPVCalQDs) (A.4) for 2 hours. The control treatment has no addition of QDs. Selected z-stack images were taken using lasers of 405 nm wavelength for the Hoechst stain, and 488 nm for the QDs and Fm4-64 membrane stain. A. The red channel displays the membrane stain, the green channel displays the QDs, and the blue channel displays the nucleus. On the left are projection images, while displayed on the right are slices taken vertically through the cell, displaying a side-view of the cell. B. Mean pixel intensity of the QDs in the cytoplasm (B.1) and nucleus (B.2) of C2C12 cells. The error bars display the S.E.M. * $p<.05$ ** $p<.01$ as determined by single factor ANOVA followed by Fisher's LSD post hoc test. Arrows display large clusters of QDs.**

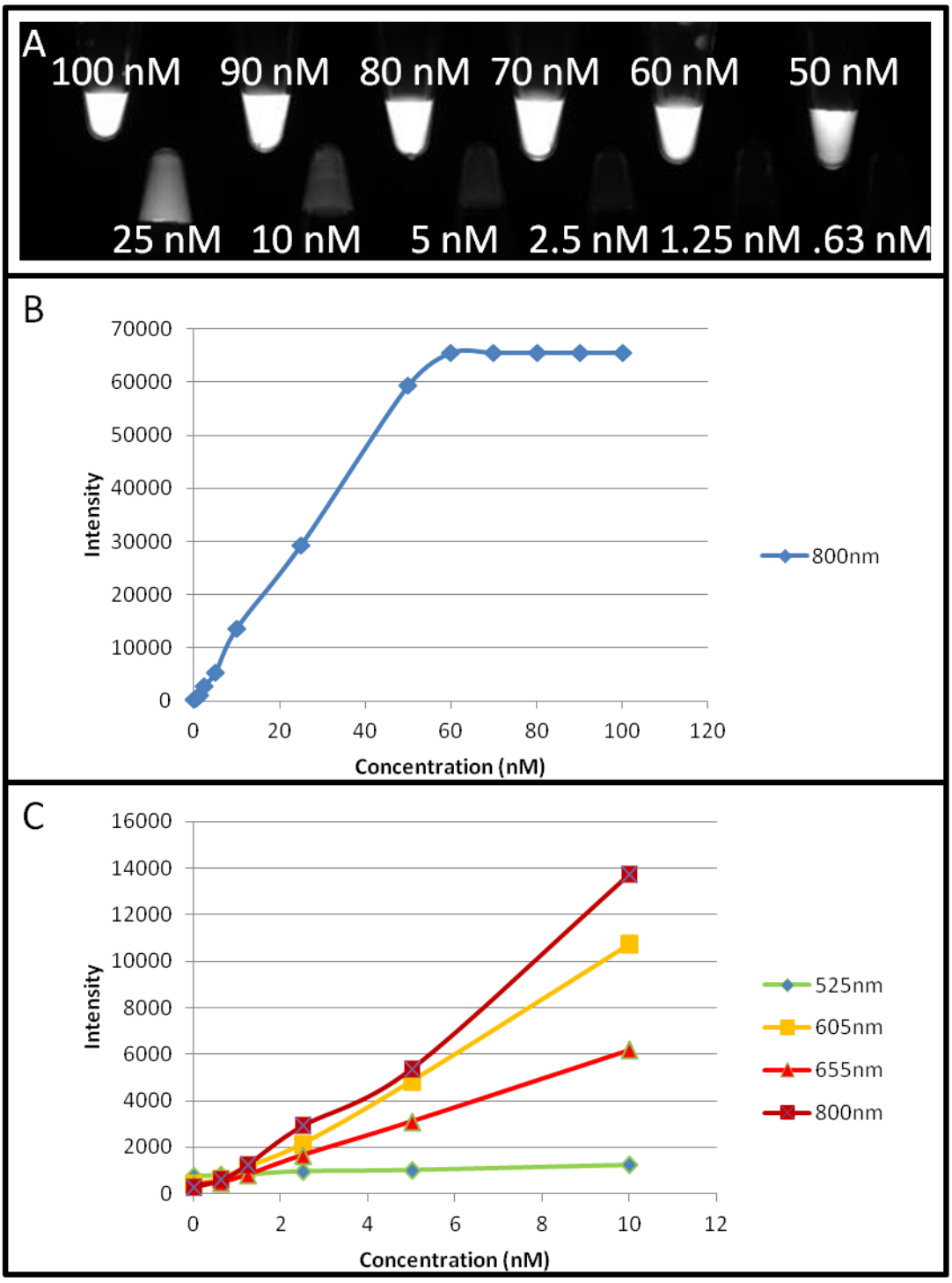
A
100 nM
90 nM
80 nM
70 nM
60 nM
50 nM
25 nM
10 nM
5 nM
2.5 nM
1.25 nM
.63 nM
B
Intensity
Concentration (nM)
800nm
C
Intensity
Concentration (nM)
525nm
605nm
655nm
800nm

Figure 4.13 Standard Curves of QDs under the IVIS Lumina. Quantum Dots at 525 nm, 605 nm, 655 nm, and 800 nm at varying concentrations were placed in microcentrifuge tubes under the IVIS Lumina. A. Image of 800 nm QDs in microcentrifuge tubes. B. Standard curve of pixel intensity of QDs in microcentrifuge tubes at 800 nm QDs from 0 to 100 nM. C. Standard curve of pixel intensity of QDs in microcentrifuge tubes at 525 nm, 605 nm, 655 nm, and 800 nm QDs from 0 to 10 nM.

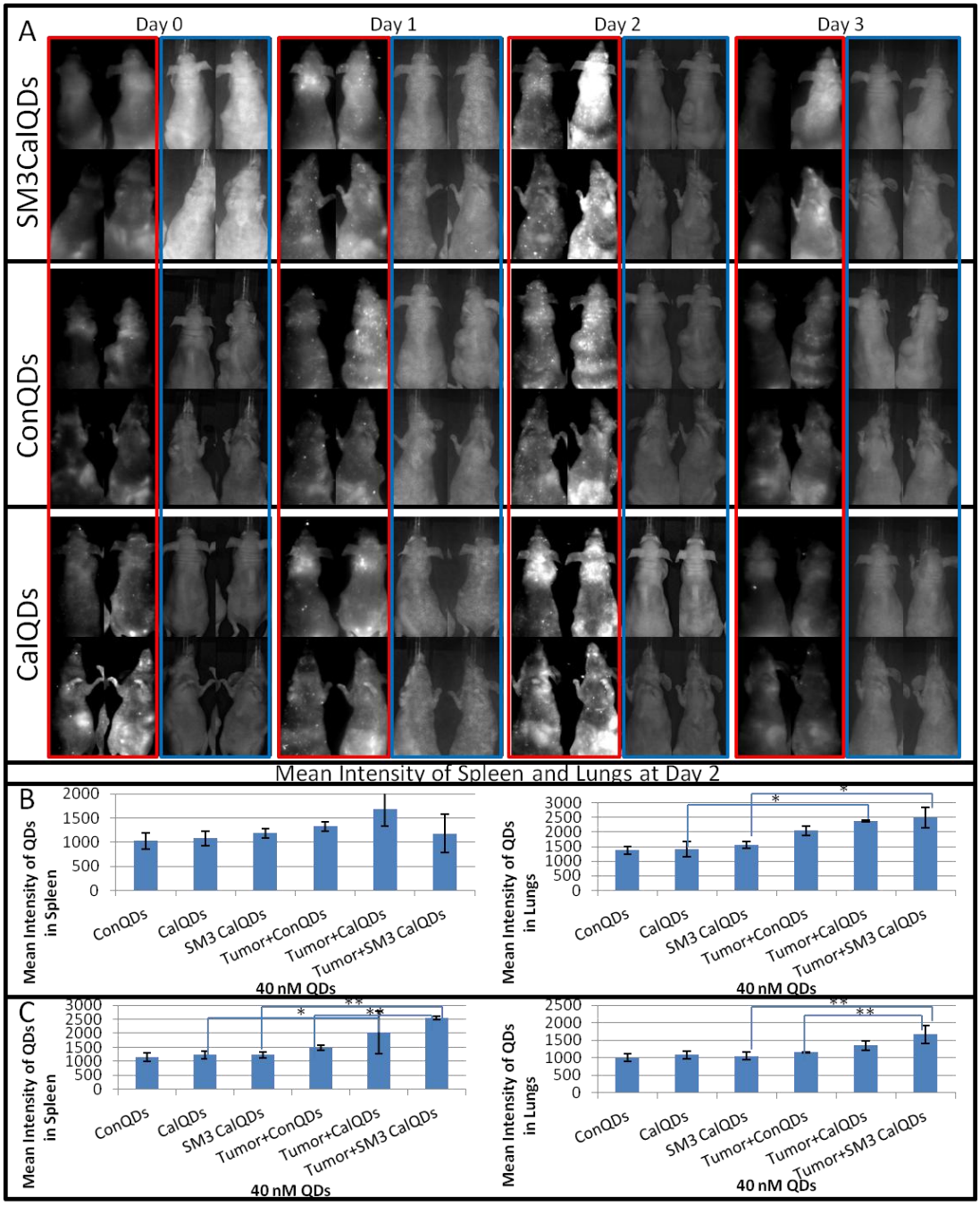
A
Day 0
Day 1
Day 2
Day 3
SM3CalQDs
ConQDs
CalQDs
Mean Intensity of Spleen and Lungs at Day 2
B
Mean Intensity of QDs in Spleen
Mean Intensity of QDs in Lungs
ConQDs
CalQDs
SM3 CalQDs
Tumor+ConQDs
Tumor+CalQDs
Tumor+SM3 CalQDs
40 nM QDs
C
Mean Intensity of QDs in Spleen
Mean Intensity of QDs in Lungs
40 nM QDs

Figure 4.14 **Over 3 Days Nude Mice with and without SUM149 Tumors Injected with 800 nm Calcitriol bound QDs conjugated with SM3 Mucin-1 antibodies (SM3CalQDs), Calcitriol bound QDs (CalQDs), and Control QDs (ConQDs). Nude Immune Deficient Mice were injected subdermally with SUM149 cells. After 6 weeks when tumors were visible, mice were tail vain injected with 100 µl 40 nM SM3CalQDs, CalQDs, or ConQDs. Mice were imaged once a day for 3 days, then sacrificed on day 4. A. There are two representative mice displayed in each treatment/day block. On the top of each block is the top view of the mice, and on the bottom is the bottom view of the mice. The mouse placed on the left has no tumor, while the one on the right has a visible tumor. In the red block are the fluorescent images for each day, and in the blue block are the visible images for each day. B. At Day 2, the mean pixel intensity of spleen and lungs in mice with and without tumors as measured from the top view of the mice. C. At Day 2, the mean pixel intensity of spleen and lungs in mice with and without tumors as measured from the bottom view of the mice. The error bars display the S.E.M. * $p<.05$ ** $p<.01$ as determined by single factor ANOVA followed by Fisher's LSD post hoc test.**

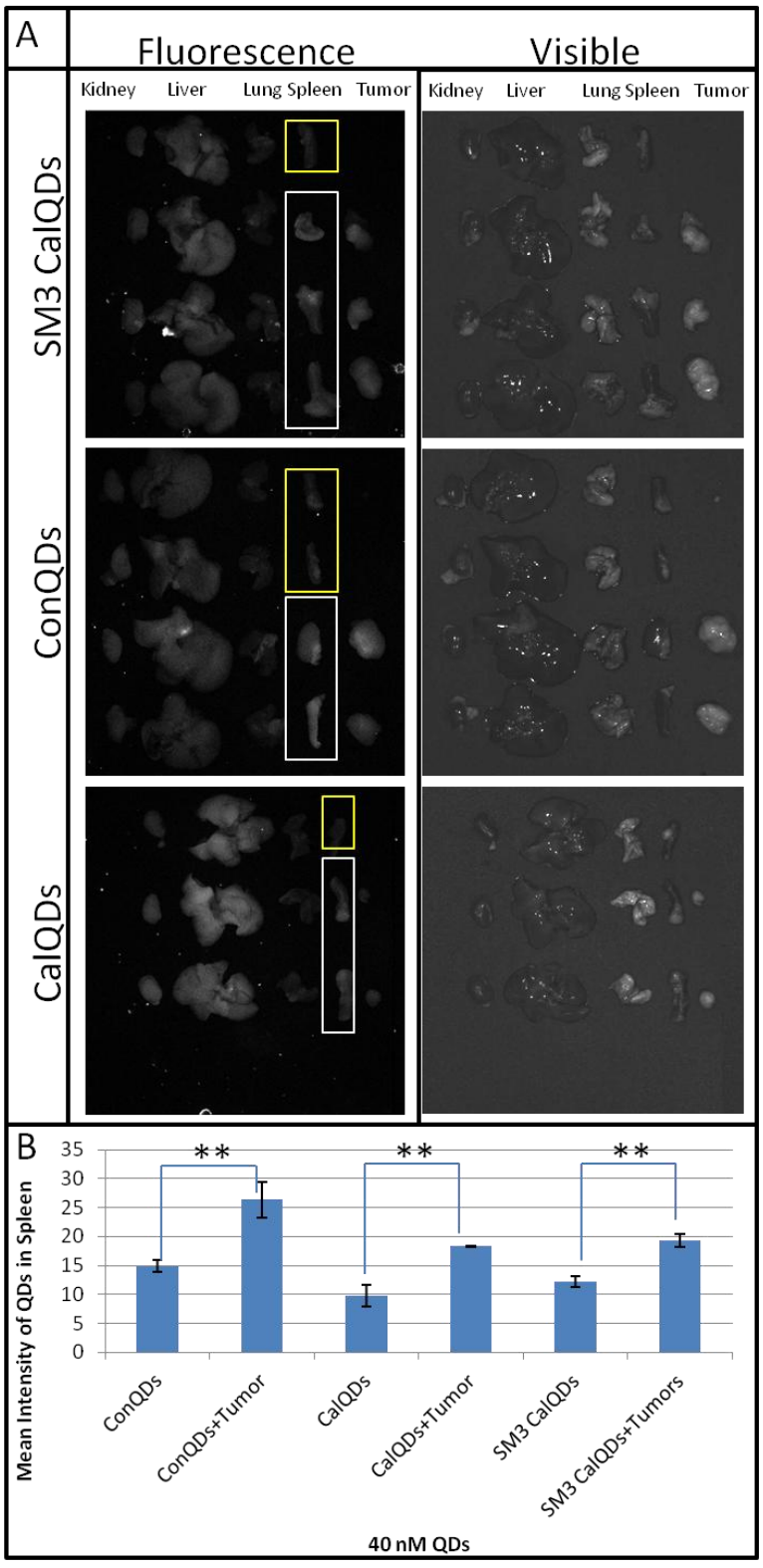
A
Fluorescence
Visible
Kidney
Liver
Lung Spleen
Tumor
SM3 CalQDs
ConQDs
CalQDs
B
Mean Intensity of QDs in Spleen
35
30
25
20
15
10
5
0
**
**
**
ConQDs
ConQDs+Tumor
CalQDs
CalQDs+Tumor
SM3 CalQDs
SM3 CalQDs+Tumors
40 nM QDs

Figure 4.15 Organs of Nude Mice with and without SUM149 Tumors Injected with Infrared 800 nm Calcitriol bound QDs conjugated with SM3 Mucin-1 antibodies (SM3 CalQDs), Calcitriol bound QDs (CalQDs), and Control QDs (ConQDs) four days previously. Over 3 Days Nude Mice with and without SUM149 Tumors Injected with Infrared 800 nm Calcitriol bound QDs conjugated with SM3 Mucin-1 antibodies (SM3CalQDs), Calcitriol bound QDs (CalQDs), and Control QDs (ConQDs). Nude Immune Deficient Mice were injected subdermally with SUM149 cells. After 6 weeks when tumors were visible, mice were tail vain injected with 100 µl 40 nM SM3CalQDs, CalQDs, or ConQDs. Mice were imaged once a day for 3 days, then sacrificed on day 4. A. Organs of the mice are displayed with control mice without tumors on top of each treatment block. On the left are the fluorescent images, and on the right are the visible images. Spleens in white squares are from mice with tumors. Spleens in yellow squares are from mice without tumors. B. The mean pixel intensity of spleens in mice with and without tumors. The error bars display the S.E.M. * p<.05 ** p<.01 as determined by single factor ANOVA followed by Fisher's LSD post hoc test.

Chapter 5

CONCLUSIONS

Direct imaging of Calcitriol has been problematic due to the lack of successful fluorescent labeling or antibodies specifically recognizing Calcitirol. For this reason, Calcitriol bound QDs were developed to image Calcitriol *in vitro* and *in vivo* [1]. Calcitriol bound QDs have a lower susceptibility to photobleaching, increased stability, broader excitation and narrow emission spectrum, and a higher signal to noise ratio than other previously developed fluorescent Calcitriol probes due to the characteristics of QDs [24-26]. Therefore, Calcitriol bound QDs can be used to visualize the location of Calcitriol and examine colocalization with other fluorescent probes. Calcitriol is crucial to human health, so it is important to perform further research to examine its large variety of essential signaling pathways. Since extensive research on Calcitriol has demonstrated that a deficiency can lead to many diseases, such as certain cancers and osteoporosis, it is essential to understand how this molecule is taken up by cells [13]. Calcitriol's role as a potential therapeutic against breast cancer has been demonstrated in clinical trials and it appears to have an effect against the metastasizing ability of Inflammatory Breast Cancer (IBC) cells [17, 22].

Calcitriol's potential as a therapeutic against IBC, a disease that has high mortality even with prompt treatment, needs to be further explored [22]. In this study, CalQDs were used as both a probe to better understand Calcitriol entry into IBC cells and as a potential targeted treatment against IBC.

Since Calcitriol is a steroid and cannot be synthesized by the cell with a fluorescent tag, not much research has been done involving direct imaging of Calcitriol. The uptake of Calcitriol into cells can now be observed through Calcitriol bound QDs [1]. Calcitriol bound QDs enter the cytoplasm and nucleus within 2 hours (Figure 4.1). Since the cytoplasm has a larger volume than the nucleus, mean intensity showing uptake is more accurate and less variable over its larger volume. Hence, 2 hour treatments of Calcitriol bound QDs were chosen, which favor observation of uptake in the cytoplasm with Calcitriol bound QDs mainly localized there at that time point.

CalQDs can be used as a probe to determine Calcitriol's method of entry into the cell. When endocytosis is prevented, decreased uptake indicates that Calcitriol does not enter the cell without endocytosis. The free hormone hypothesis states that since Calcitriol is hydrophobic, it must enter the cell via diffusion through the plasma membrane [31]. However, Calcitriol is hydrophilic in serum when bound to the Vitamin D binding protein, and associates closely with caveolae [3, 36, 37]. Its precursor, 25-hydroxy-vitamin D3 has been shown to enter the kidney proximal tubule cells through clathrin mediated endocytosis [47]. Calcitriol's method of uptake into the cell has not been tested. Calcitriol has been shown to be particularly effective

against Inflammatory Breast Cancer cells and emboli [22]. Caveolae are over-expressed in IBC cells, so if caveolae function is essential to Calcitriol uptake, then the ability of Calcitriol to treat Inflammatory Breast Cancer cells would depend on the caveolae expression [44]. The over-expression may even contribute to Calcitriol's ability to impact the metastasizing properties of SUM149 cells, but not significantly affect the non-inflammatory MDA-MB-231 cells [22].

Two main forms of endocytosis, caveolae and clathrin coated pits, were disrupted in SUM149 IBC cells. Calcitriol bound QDs were shown to have decreased uptake in the cytoplasm and nucleus of SUM149 cells when caveolae or clathrin coated pits are disrupted (Figure 4.4-6). This is confirmed by a decreased biological response in cells with disrupted caveolae or clathrin coated pits (Figure 4.7). Both endocytotic structures appear to be necessary for normal levels of Calcitriol uptake into the cell, so it is possible that Calcitriol enters the cell via both endocytotic pathways. For example, a peptide, TAMRA-claudin-1, enters cells via both clathrin and caveolae mediated endocytosis [53].

Although the decreased uptake in SUM149 cells resulting from disrupting caveolae or clathrin coated pits indicates that both structures are used for endocytosis, the uptake was brought down to the level of QD uptake even when only one type of endocytotic structure was disrupted (Figure 4.4-6). This indicates that there was little to no uptake of Calcitriol when either caveolae or clathrin coated pits were disrupted, which would not be the case if both structures are used for endocytosis. Caveolae are independent structures from clathrin coated pits, so there would only be a partial

decrease when one was knocked out. It is possible that Calcitriol requires both structures to be functional, but is only endocytosed by one type. Calcitriol must colocalize with the structures to be endocytosed. In skeletal muscle cells, VDR colocalizes with caveolae when Calcitriol is a ligand for caveolae [36, 37]. This is an indication that Calcitriol entry is possible at the caveolae. Without colocalization, it's more likely that the membrane structures are involved in upstream signaling necessary for uptake rather than in the uptake itself. Colocalization between VDR, caveolae, and Calcitriol was examined in SUM149 cells. Like the skeletal muscle cells, there was an increase in correlation and colocalization between VDR and caveolae after Calcitriol was added (Figure 4.8). There was also a correlation and colocalization between caveolae and Calcitriol and between VDR and Calcitriol indicating a colocalization between all three after Calcitriol enters the cell at the caveolae (Figure 4.8). The same association was examined between clathrin coated pits, VDR, and Calcitriol. If Calcitriol enters the cell at the clathrin coated pits, colocalization would be a good indicator for this occurrence. However, while there was an increase in correlation between VDR and clathrin coated pits, the colocalization did not increase in response to Calcitriol. Also, both correlation and colocalization remained very low between clathrin coated pits and Calcitriol and between VDR and Calcitriol (Figure 4.9).

It is likely that while the function of clathrin coated pits is necessary for Calcitriol uptake, that Calcitriol does not actually use that form of endocytosis to enter, since it does not colocalize with clathrin. Beta-arrestin-2 increases the activity of RXR for downstream signaling [7]. Beta arrestins act as adapters that connect

receptors to clathrin mediated endocytsosis, while also acting as signaling scaffolds for MAPKs [8]. Receptor-beta-arrestin complexes bind to ap-2 in clathrin coated pits [7]. Disruption of clathrin coated pits may lower the activity of RXR, with a potential decrease in beta-arrestin activity (Figure 5.1). RXR activity is necessary for nuclear uptake of CalQDs [3, 9], and decreased activity may have caused the observed decreased nuclear uptake of CalQDs when SUM149 cells were treated with EH29 (Figure 5.1). RXR may be involved in Calcitriol's membrane docking, causing its function to also be required for cytoplasmic uptake. To examine this, future work examining RXR activity can be explored. CalQD uptake can be examined after knockdown of RXR. While it is likely that Calcitriol does not enter via clathrin mediated endocytosis, with the demonstrated colocalization between Calcitriol and Caveolae and the dependence on CAV-1 expression for uptake it is possible that Calcitriol is uptaken via caveolae (Figure 5.1). However, since caveolae acts as a signaling scaffold, it is also likely that its role as a scaffold is what allows Calcitriol to be uptaken, such as the interaction of CAV-1 with VDR in skeletal muscle cells [36, 37]. The free hormone hypothesis cannot be refuted with this study, but further research should be performed on the role of caveolae and clathrin coated pits in the uptake of caveolae, since this research has demonstrated that the function of both structures are necessary [31].

Healthy serum levels of Calcitriol that do not lead to hypercalcemia are at 0.12 nM, which is much lower than the 100 nM necessary to affect the metastasizing ability of IBC cells and their ability to form emboli [18, 22]. In order to reach a high enough

concentration at a tumor site *in vivo*, mucin-1 (MUC-1) antibodies were conjugated to Calcitriol bound QDs. The SM3 clone of MUC-1 can be used to directly target Calcitriol bound QDs to IBC cells [49]. The MUC-1 conjugated CalQDs were taken up by human IBC SUM149 cells at a slightly higher concentration, but at a significantly lower concentration in the mouse C2C12 cell line (Figure 4.10, 4.12). So, they appear to target human IBC cells more than the control mouse cell line. They also induced biological activity in SUM149 cells as well as Calcitriol and CalQDs (Figure 4.11). This success *in vitro* indicated that they were successfully conjugated in a way that they could be targeted to the IBC cells with their biological activity intact. When the SM3 CalQDs were used *in vivo*, in mice with tumors they appeared to be targeted to the lungs, where the IBC cells often metastasize [22] and to the spleen, which was the closest organ of the lymphatic system to the original subcutaneous injection site where the large IBC tumors are located (Figure 4.14-5). The SM3 CalQDs appeared to remain in the system longer than CalQDs, as the fluorescent intensity was greater in those tumor laden mice treated with SM3 CalQDs at day 3 (Figure 4.14A). However, the large tumors did not appear to be targeted (Figure 4.14A). It is possible that only the outside of the large tumors could be targeted, and would cause them to be less fluorescent. However there was a clear difference in SM3 CalQD distribution and Control QD distribution, which indicates that further exploration of this molecule *in vivo* is warranted (Figure 4.14).

The results indicate that CalQDs were successful as both a probe into Calcitriol uptake in IBC cells and as a potential method to target Calcitriol directly to IBC cells.

Additional research into the mechanism behind CalQD uptake and their viability *in vivo* is necessary to make further conclusions. The unique CalQD molecule can also be expanded for use beyond Inflammatory Breast Cancer with Calcitriol's major role in maintaining health and as a therapeutic. With this probe, the current understanding of Vitamin D biology can be expanded and could lead to improvements in therapy for both Vitamin D deficient diseases and cancers [2].

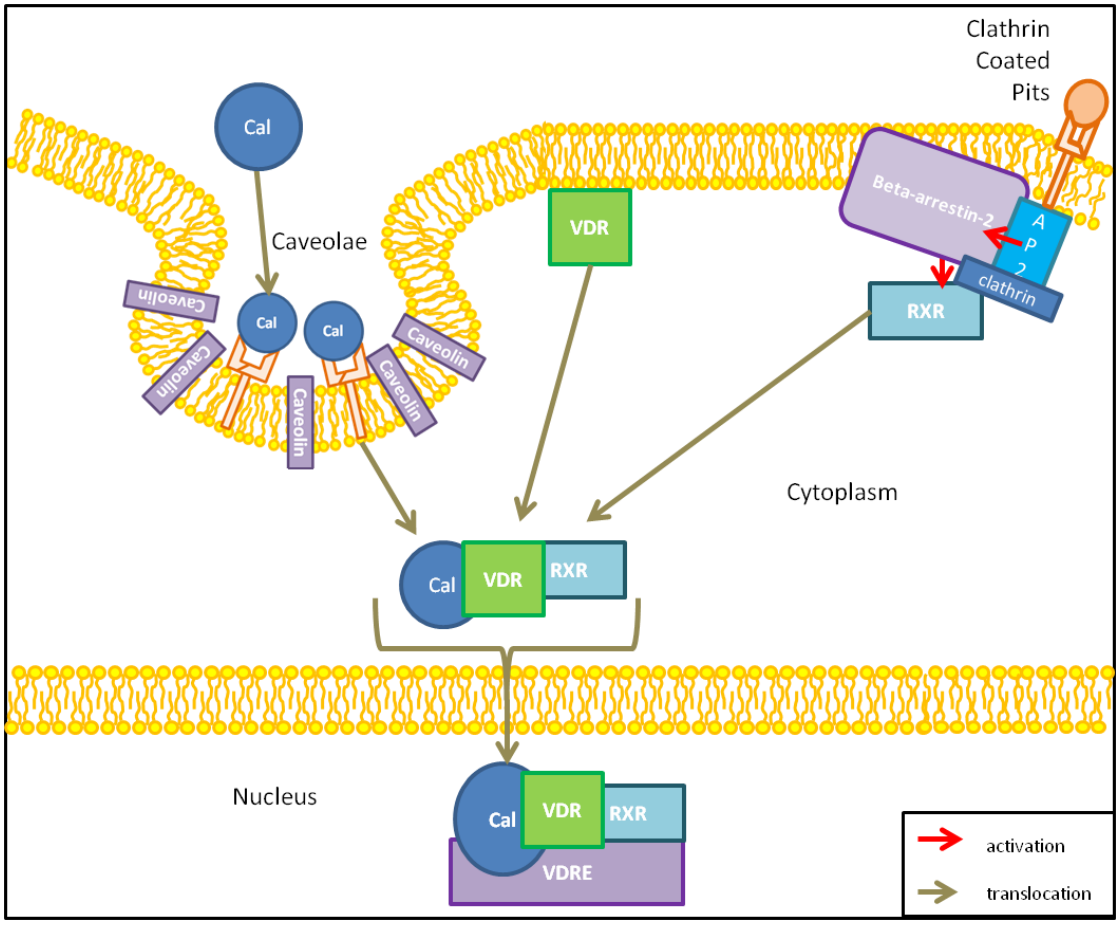

Figure 5.1 Uptake of Calcitriol at the Caveolae. This study has determined that Calcitriol colocalizes with caveolae, and the function of clathrin coated pits and caveolae are necessary for cytoplasmic and nuclear uptake. Our model derived from our data shows that after associating with caveolae, and being uptaken into the cell, Vitamin D Receptor (VDR) translocates from the nucleus and binds to Calcitriol. RXR receptor is activated by beta-arrestin-2, which is bound to AP-2 at clathrin coated pits, and binds to VDR, forming a heterodimer. The heterodimer translocates to the nucleus to interact with the Vitamin D Response Elements (VDRE) to induce or repress transcription.

REFERENCES

1. Bonor, J., R. Schaefer, N. Menegazzo, K. Booksh, and A. Nohe, *Design of 1,25 Dihydroxyvitamin D3 Coupled Quantum Dots, a Novel Imaging Tool* J. Nanosci. Nanotechnol., 2012. **12**: p. 2185-2191.

2. Haroon, M. and M.J. Regan, *Vitamin D deficiency: the time to ignore it has passed.* Int J Rheum Dis. **13**(4): p. 318-23.

3. Lehmann, B. and M. Meurer, *Vitamin D metabolism.* Dermatol Ther. **23**(1): p. 2-12.

4. Bikle, D.D., *Vitamin D: an ancient hormone.* Exp Dermatol, 2010. **20**(1): p. 7-13.

5. Richard, C.L., M.C. Farach-Carson, B. Rohe, I. Nemere, and K.A. Meckling, *Involvement of 1,25D3-MARRS (membrane associated, rapid response steroid-binding), a novel vitamin D receptor, in growth inhibition of breast cancer cells.* Exp Cell Res. **316**(5): p. 695-703.

6. Tudpor, K., J. Teerapornpuntakit, W. Jantarajit, N. Krishnamra, and N. Charoenphandhu, *1,25-dihydroxyvitamin D(3) rapidly stimulates the solvent drag-induced paracellular calcium transport in the duodenum of female rats.* J Physiol Sci, 2008. **58**(5): p. 297-307.

7. Piu, F., N.K. Gauthier, and F. Wang, *Beta-arrestin 2 modulates the activity of nuclear receptor RAR beta2 through activation of ERK2 kinase.* Oncogene, 2006. **25**(2): p. 218-29.

8. Luttrell, L.M. and R.J. Lefkowitz, *The role of b-arrestins in the termination and transduction of G-protein-coupled receptor signals.* Journal of Cell Science, 2002. **115**: p. 455-465.

9. Lefebvre, P., Y. Benomar, and B. Staels, *Retinoid X receptors: common heterodimerization partners with distinct functions.* Trends Endocrinol Metab, 2010. **21**(11): p. 676-83.

10. Lisse, T.S., T. Liu, M. Irmler, J. Beckers, H. Chen, J.S. Adams, and M. Hewison, *Gene targeting by the vitamin D response element binding protein reveals a role for vitamin D in osteoblast mTOR signaling.* FASEB J. **25**(3): p. 937-47.

11. Valdivielso, J.M., *The physiology of vitamin D receptor activation.* Contrib Nephrol, 2009. **163**: p. 206-12.

12. Jensen, S.S., M.W. Madsen, J. Lukas, L. Binderup, and J. Bartek, *Inhibitory effects of 1alpha,25-dihydroxyvitamin D(3) on the G(1)-S phase-controlling machinery.* Mol Endocrinol, 2001. **15**(8): p. 1370-80.

13. Adams, J.S. and M. Hewison, *Update in vitamin D.* J Clin Endocrinol Metab, 2010. **95**(2): p. 471-8.

14. Pierrot-Deseilligny, C. and J.C. Souberbielle, *Widespread vitamin D insufficiency: A new challenge for primary prevention, with particular reference to multiple sclerosis.* Presse Med, 2011. **40**(4 Pt 1): p. 349-56.

15. Tuohimaa, P., T. Keisala, A. Minasyan, J. Cachat, and A. Kalueff, *Vitamin D, nervous system and aging.* Psychoneuroendocrinology, 2009. **34 Suppl 1**: p. S278-86.

16. Nordin, B.E., *Evolution of the calcium paradigm: the relation between vitamin D, serum calcium and calcium absorption.* Nutrients, 2010. **2**(9): p. 997-1004.

17. Krishnan, A.V. and D. Feldman, *Mechanisms of the anti-cancer and anti-inflammatory actions of vitamin D.* Annu Rev Pharmacol Toxicol, 2011. **51**: p. 311-36.

18. Breslau, N.A., J.L. McGuire, J.E. Zerwekh, E.P. Frenkel, and C.Y. Pak, *Hypercalcemia associated with increased serum calcitriol levels in three patients with lymphoma.* Ann Intern Med, 1984. **100**(1): p. 1-6.

19. Zhang, H., Q.R. Huang, J.M. Gu, W.W. Hu, Y.J. Liu, Y.Q. Hu, and Z.L. Zhang, *Comparison of the effects of cholecalciferol and calcitriol on calcium metabolism and bone turnover in Chinese postmenopausal women with vitamin D insufficiency.* Acta Pharmacol Sin, 2012. **33**(4): p. 490-5.

20. Dushkin, H. and M. Cristofanilli, *Inflammatory breast cancer.* J Natl Compr Canc Netw. **9**(2): p. 233-40; quiz 241.

21. Robertson, F.M., M. Bondy, W. Yang, H. Yamauchi, S. Wiggins, S. Kamrudin, S. Krishnamurthy, H. Le-Petross, L. Bidaut, A.N. Player, S.H. Barsky, W.A. Woodward, T. Buchholz, A. Lucci, N.T. Ueno, and M. Cristofanilli, *Inflammatory breast cancer: the disease, the biology, the treatment.* CA Cancer J Clin, 2010. **60**(6): p. 351-75.

22. Hillyer, R.L., P. Sirinvasin, M. Joglekar, R.A. Sikes, K.L. Van Golen, and A. Nohe, *Differential effects of vitamin D treatment on inflammatory and non-inflammatory breast cancer cell lines.* Clin Exp Metastasis, 2012.

23. Barsony, J., I. Renyi, W. McKoy, H.C. Kang, R.P. Haugland, and C.L. Smith, *Development of a biologically active fluorescent-labeled calcitriol and its use to study hormone binding to the vitamin D receptor.* Anal Biochem, 1995. **229**(1): p. 68-79.

24. Derfus, C., Bhatia, *Probing the Cytoxicity of Semiconductor Quantum Dots.* Nano Letters, 2004. **4**(1): p. 11-18.

25. Alivisatos, A.P., W. Gu, and C. Larabell, *Quantum dots as cellular probes.* Annu Rev Biomed Eng, 2005. **7**: p. 55-76.

26. Barroso, M.M., *Quantum dots in cell biology.* J Histochem Cytochem. **59**(3): p. 237-51.

27. Whitesides, G.M., *The 'right' size in nanobiotechnology.* Nat Biotechnol, 2003. **21**(10): p. 1161-5.

28. Hardman, R., *A toxicologic review of quantum dots: toxicity depends on physicochemical and environmental factors.* Environ Health Perspect, 2006. **114**(2): p. 165-72.

29. *1,3-cyclohexanediol*, in *American Chemical Society*. 2011.

30. *cyclohexanol*, in *American Chemical Society*. 2011.

31. Willnow, T.E. and A. Nykjaer, *Cellular uptake of steroid carrier proteins--mechanisms and implications.* Mol Cell Endocrinol, 2009. **316**(1): p. 93-102.

32. Sandvig, K., S. Pust, T. Skotland, and B. van Deurs, *Clathrin-independent endocytosis: mechanisms and function.* Curr Opin Cell Biol, 2011. **23**(4): p. 413-20.

33. Kiss, A.L. and E. Botos, *Endocytosis via caveolae: alternative pathway with distinct cellular compartments to avoid lysosomal degradation?* J Cell Mol Med, 2009. **13**(7): p. 1228-37.

34. Staubach, S. and F.G. Hanisch, *Lipid rafts: signaling and sorting platforms of cells and their roles in cancer.* Expert Rev Proteomics, 2011. **8**(2): p. 263-77.

35. Rodal, S.K., G. Skretting, O. Garred, F. Vilhardt, B. van Deurs, and K. Sandvig, *Extraction of cholesterol with methyl-beta-cyclodextrin perturbs formation of clathrin-coated endocytic vesicles.* Mol Biol Cell, 1999. **10**(4): p. 961-74.

36. Boland, R.L., *VDR activation of intracellular signaling pathways in skeletal muscle.* Mol Cell Endocrinol, 2011. **347**(1-2): p. 11-6.

37. Buitrago, C. and R. Boland, *Caveolae and caveolin-1 are implicated in 1alpha,25(OH)2-vitamin D3-dependent modulation of Src, MAPK cascades and VDR localization in skeletal muscle cells.* J Steroid Biochem Mol Biol, 2010. **121**(1-2): p. 169-75.

38. Pancotti, F., L. Roncuzzi, M. Maggiolini, and A. Gasperi-Campani, *Caveolin-1 silencing arrests the proliferation of metastatic lung cancer cells through the inhibition of STAT3 signaling.* Cell Signal, 2012. **24**(7): p. 1390-7.

39. Masuelli, L., A. Budillon, L. Marzocchella, M.A. Mrozek, D. Vitolo, E. Di Gennaro, S. Losito, P. Sale, F. Longo, F. Ionna, F. Lista, R. Muraro, A. Modesti, and R. Bei, *Caveolin-1 overexpression is associated with simultaneous abnormal expression of the E-cadherin/alpha-beta catenins complex and multiple ErbB receptors and with lymph nodes metastasis in head and neck squamous cell carcinomas.* J Cell Physiol, 2011.

40. Kuo, S.R., S.A. Tahir, S. Park, T.C. Thompson, S. Coffield, A.E. Frankel, and J.S. Liu, *Anti-caveolin-1 Antibodies As Anti-Prostate Cancer Therapeutics.* Hybridoma (Larchmt), 2012. **31**(2): p. 77-86.

41. Wu, K.N., M. Queenan, J.R. Brody, M. Potoczek, F. Sotgia, M.P. Lisanti, and A.K. Witkiewicz, *Loss of stromal caveolin-1 expression in malignant melanoma metastases predicts poor survival.* Cell Cycle, 2011. **10**(24): p. 4250-5.

42. Aoki, M.N., M.K. Amarante, J.M. Oda, and M.A. Watanabe, *Caveolin involvement and modulation in breast cancer.* Mini Rev Med Chem, 2011. **11**(13): p. 1143-52.

43. Thompson, D.E., M.D. Siwicky, and R.A. Moorehead, *Caveolin-1 expression is elevated in claudin-low mammary tumor cells.* Cancer Cell Int, 2012. **12**: p. 6.

44. Van den Eynden, G.G., S.J. Van Laere, I. Van der Auwera, S.D. Merajver, E.A. Van Marck, P. van Dam, P.B. Vermeulen, L.Y. Dirix, and K.L. van Golen, *Overexpression of caveolin-1 and -2 in cell lines and in human samples of inflammatory breast cancer.* Breast Cancer Res Treat, 2006. **95**(3): p. 219-28.

45. Ramanan, V., N.J. Agrawal, J. Liu, S. Engles, R. Toy, and R. Radhakrishnan, *Systems biology and physical biology of clathrin-mediated endocytosis.* Integr Biol (Camb), 2011. **3**(8): p. 803-15.

46. Suksanpaisan, L., T. Susantad, and D.R. Smith, *Characterization of dengue virus entry into HepG2 cells.* J Biomed Sci, 2009. **16**: p. 17.

47. Kaseda, R., M. Hosojima, H. Sato, and A. Saito, *Role of megalin and cubilin in the metabolism of vitamin D(3).* Ther Apher Dial, 2011. **15 Suppl 1**: p. 14-7.

48. Burke, P.A., J.P. Gregg, B. Bakhtiar, L.A. Beckett, G.L. Denardo, H. Albrecht, R.W. De Vere White, and S.J. De Nardo, *Characterization of MUC1 glycoprotein on prostate cancer for selection of targeting molecules.* Int J Oncol, 2006. **29**(1): p. 49-55.

49. Burchell, J.M., A. Mungul, and J. Taylor-Papadimitriou, *O-linked glycosylation in the mammary gland: changes that occur during malignancy.* J Mammary Gland Biol Neoplasia, 2001. **6**(3): p. 355-64.

50. Beatty, P.L., S.E. Plevy, A.R. Sepulveda, and O.J. Finn, *Cutting edge: transgenic expression of human MUC1 in IL-10-/- mice accelerates inflammatory bowel disease and progression to colon cancer.* J Immunol, 2007. **179**(2): p. 735-9.

51. Zou, M., F. Zhang, J. Li, and N. Wang, *Rapid detection of lily symptomless virus with CdTe quantum dots by flow cytometry.* J Immunoassay Immunochem, 2011. **32**(4): p. 259-68.

52. Costes, S.V., D. Daelemans, E.H. Cho, Z. Dobbin, G. Pavlakis, and S. Lockett, *Automatic and quantitative measurement of protein-protein colocalization in live cells.* Biophys J, 2004. **86**(6): p. 3993-4003.

53. Zwanziger, D., C. Staat, A.V. Andjelkovic, and I.E. Blasig, *Claudin-derived peptides are internalized via specific endocytosis pathways.* Ann N Y Acad Sci, 2012. **1257**(1): p. 29-37.

Appendix A

PERMISSION TO PERFORM ANIMAL RESEARCH ANNUAL RENEWAL OF PROTOCOL

University of Delaware
Institutional Animal Care and Use Committee
Annual Review

RECEIVED
JUN 23 2011
IACUC

(Please complete below using Arial, size 12 Font.)

Title of Protocol: Studying the Distribution Storage of Nanoparticles in Female Mice

AUP Number: 1199-2011-2 ← **(4 digits only)**

Principal Investigator: Dr. Anja Nohe

Common Name: Mouse

Genus Species: *Mus musculus*

Pain Category: ***(please mark one)***

USDA PAIN CATEGORY: *(Note change of categories from previous form)*

Category	Description
☐ B	Breeding or holding where NO research is conducted
X C	Procedure involving momentary or no pain or distress
☐ D	Procedure where pain or distress is alleviated by appropriate means (analgesics, tranquilizers, euthanasia etc.)
☐ E	Procedure where pain or distress cannot be alleviated, as this would adversely affect the procedures, results or interpretation

Official Use Only

IACUC Approval Signature: _____

Date of Approval: 6/24/2011

Principal Investigator Assurance

1. I agree to abide by all applicable federal, state, and local laws and regulations, and UD policies and procedures.
2. I understand that deviations from an approved protocol or violations of applicable policies, guidelines, or laws could result in immediate suspension of the protocol and may be reportable to the Office of Laboratory Animal Welfare (OLAW).
3. I understand that the Attending Veterinarian or his/her designee must be consulted in the planning of any research or procedural changes that may cause more than momentary or slight pain or distress to the animals.
4. I declare that all experiments involving live animals will be performed under my supervision or that of another qualified scientist listed on this AUP. All listed personnel will be trained and certified in the proper humane methods of animal care and use prior to conducting experimentation.
5. I understand that emergency veterinary care will be administered to animals showing evidence of discomfort, ailment, or illness.
6. I declare that the information provided in this application is accurate to the best of my knowledge. If this project is funded by an extramural source, I certify that this application accurately reflects all currently planned procedures involving animals described in the proposal to the funding agency.
7. I assure that any modifications to the protocol will be submitted to the UD-IACUC and I understand that they must be approved by the IACUC prior to initiation of such changes.
8. I understand that the approval of this project is for a maximum of one year from the date of UD-IACUC approval and that I must re-apply to continue the project beyond that period.
9. I understand that any unanticipated adverse events, morbidity, or mortality must be reported to the UD-IACUC immediately.
10. I assure that the experimental design has been developed with **consideration of the three Rs: reduction, refinement, and replacement, to reduce animal pain and/or distress and the number of animals used in the laboratory.**
11. I assure that the proposed research does not unnecessarily duplicate previous experiments. *(Teaching Protocols Exempt)*
12. I understand that by signing, I agree to these assurances. Signature of Principal Investigator — Date: June 1, 2011

SIGNATURE(S) OF ALL PERSONS LISTED ON THIS PROTOCOL

I certify that I have read this protocol, accept my responsibility and will perform only the procedures that have been approved by the IACUC.

Name	Signature
1. Anja Nohe	
2. Beth Bragdon	
3. Jillian Hash	
4.	
5.	
6.	
7.	
8.	
9.	
10.	
11.	
12.	
13.	
14.	
15.	

IACUC approval of animal protocols must be renewed on an annual basis.

1. **Previous Approval Date:** 6/30/2010

   Is Funding Source the same as on original, approved AUP?

   X Yes ☐ **No**

   If no, please state Funding Source and Award Number:

2. **Record of Animal Use:**

Common Name	Genus Species	Total Number Previously Approved	Number Used To Date
1. Mouse	*Mus musculus*	208	0
2.			
3.			
4.			
5.			

3. **Protocol Status:** *(Please indicate by check mark the status of project.)*

   Request for Protocol Continuance:

   ☐ A. Active: Project ongoing

   ☐ B. Currently inactive: Project was initiated but is presently inactive

   X C. Inactive: Project never initiated but anticipated starting date is: Summer 2011

   Request for Protocol Termination:

   ☐ D. Inactive: Project never initiated

   ☐ E. Completed: No further activities with animals will be done.

4. **Project Personnel:** Have there been any personnel changes since the last IACUC approval? X Yes ☐ No

   If Yes, fill out the Amendment to Add/Delete Personnel form to "Add" Personnel.

Project Personnel Deletions:

Name	Effective Date
1. Suranjit Mukherjee	6/1/2011
2.	
3.	
4.	
5.	

5. Progress Report: If the status of this project is 3.A or 3.B, please provide a brief update on the progress made in achieving the aims of the protocol.

N/A

6. Problems or Adverse Effects: If the status of this project is 3.A or 3.B, please describe any unanticipated adverse events, morbidity, or mortality, the cause if known, and how these problems were resolved. If there were none, this should be indicated.

N/A

Appendix B

PERMISSION TO PERFORM ANIMAL RESEARCH AMENDMENT TO ADD PERSONNEL

University of Delaware
Institutional Animal Care and Use Committee
Request to Amend An Animal Use Protocol
AMENDMENT TO ADD PERSONNEL

RECEIVED
JAN 17 2012
IACUC

(Please complete below using Arial, size 12 Font.)

Title of Protocol: Studying the Distribution Storage of Nanoparticles in Female Mice	
AUP Number: 1199-2012-AP	← **(4 digits only)**
Principal Investigator: Anja Nohe	
Common Name: Mouse **Genus Species:** Mus Musculus	
Category Assigned: *(please mark one)* X A. None to slight or momentary pain or distress ☐ B. Pain or distress will be alleviated by drugs or other means ☐ C. Pain or distress will not be alleviated	
IACUC approval of major changes to an animal protocol must be reviewed and approved prior to initiating the work.	

Official Use Only

IACUC Approval Signature: _____

Date of Approval: 1/23/2012

Certification Statement

1. I understand that all use of animals or animal tissues must have prior IACUC approval. I understand that unauthorized animal use is reportable to the Office of Laboratory Animal Welfare (OLAW).

2. I certify that this form accurately describes all aspects of the proposed animal usage and that the proposed work is not unnecessarily duplicative.

3. I accept responsibility for ensuring that all personnel working on this project are aware of, and will not deviate from, the IACUC approved procedures outlined on this form, that they will adhere to the regulations regarding the humane treatment of laboratory animals and that they will receive proper training.

4. I understand that if I (or contact personnel listed on this form) cannot be contacted and animals on this project show evidence of illness or pain, emergency care, including euthanasia may be administered at the discretion of the attending veterinarian.

5. I understand that the approval is not final until I receive notification of such, and that the IACUC can recommend or require changes to the protocol.

6. I have completed the Animal Facility Safety Training for working with animals, and the required certification for this training is up to date and on file in the animal facility. My personnel listed on this form also have current certification on file, or will be certified before starting work.

7. If survival surgical procedures or post-operative recovery are to be performed outside the animal facility, this site has been inspected and approved by the attending veterinarian.

8. I understand that approval of projects is for a maximum of one year from the date of IACUC approval and I must re-apply to continue the project beyond that period. I understand that any significant changes in procedures must be approved by the IACUC prior to implementation.

9. I certify that everyone listed on this protocol has read it and has signed it.

Signature of Principal Investigator

12/21/11
Date

SIGNATURE(S) OF ALL PERSONS LISTED ON THIS PROTOCOL

I certify that I have read this protocol, accept my responsibility and will perform only the procedures that have been approved by the IACUC.

Name	Signature
1. Ken Van Golen	
2. Jeremy Bonor	
3. Rachel Schaefer	
4.	
5.	
6.	
7.	
8.	
9.	
10.	
11.	
12.	
13.	
14.	
15.	

experience with proposed species. Indicate status: Post-Doc, Ph.D., Graduate, Undergraduate, Student, Technician, etc. If no experience, list who will train.)

Name	Home Phone Number	Office Phone Number	Received Animal Facility Training	
			Yes	No
1. Jeremy Bonor	302-690-1350	302-831-8732	X	

Status: Technician

Qualifications: 4 years of experience working with mice – euthanized mice with carbon dioxide and thereafter. performed cervical dislocation. Has experience with intravenous tail vain injections.

Responsibilities: Will perform injections with the assistance of Dr. Van Golen.

Name	Home Phone Number	Office Phone Number	Received Animal Facility Training	
			Yes	No
2. Rachel Schaefer	302-525-4685	302-419-8234	X	

Status: Graduate Student

Qualifications: No previous experience with mice, will be trained with sterile technique with immunocompromised mice by Frank Warren. Has been trained on the Caliper PerkinElmer VivoVision IVIS Lumina with XGI-8 Gas Anesthesia.

Responsibilities: Will transport mice to the barrier facility and examine using the Caliper PerkinElmer VivoVision IVIS Lumina with XGI-8 Gas Anesthesia.